



Holocene occupation of the Andean highlands: a new radiocarbon chronology for the Telarmachay rockshelter (Central Andes, Peru)

Manon Le Neün, Elise Dufour, Antoine Zazzo, Olivier Tombret, François Thil,
Jane Wheeler, Thomas Cucchi, Nicolas Goepfert

► To cite this version:

Manon Le Neün, Elise Dufour, Antoine Zazzo, Olivier Tombret, François Thil, et al.. Holocene occupation of the Andean highlands: a new radiocarbon chronology for the Telarmachay rockshelter (Central Andes, Peru). *Quaternary Science Reviews*, 2023, 312, pp.108146. 10.1016/j.quascirev.2023.108146 . hal-04135375

HAL Id: hal-04135375

<https://hal.science/hal-04135375>

Submitted on 20 Jun 2023

HAL is a multi-disciplinary open access archive for the deposit and dissemination of scientific research documents, whether they are published or not. The documents may come from teaching and research institutions in France or abroad, or from public or private research centers.

L'archive ouverte pluridisciplinaire **HAL**, est destinée au dépôt et à la diffusion de documents scientifiques de niveau recherche, publiés ou non, émanant des établissements d'enseignement et de recherche français ou étrangers, des laboratoires publics ou privés.



Distributed under a Creative Commons Attribution 4.0 International License

« CC-BY 4.0 », <https://creativecommons.org/licenses/by/4.0/>, Distributed under a Creative Commons Attribution | 4.0 International licence.

This research was funded, in whole or in part, by [the Région Île-de-France and the Domaine d'Intérêt Majeur “Matériaux anciens et patrimoniaux” (DIM-MAP, AAP 2018-3, project CAMELIDOM), the Action Transversale du Muséum (ATM CHRONOCAM) and Ecole Doctorale 227 “Sciences de la nature et de l'Homme: évolution et écologie” of the Muséum national d'Histoire naturelle and Sorbonne Université (ED227 MNHN-SU, France) and ANR CAMELANDES (ANR, Grant # -15-CE27-0002-01)]. A CC-BY public copyright license has been applied by the authors to the present document and will be applied to all subsequent versions up to the Author Accepted Manuscript arising from this submission, in accordance with the grant's open access conditions.

**Title: Holocene occupation of the Andean highlands: a new radiocarbon chronology for
the Telarmachay rockshelter (Central Andes, Peru)**

Authors:

Manon Le Neün^{1*}, Elise Dufour¹, Antoine Zazzo¹, Olivier Tombret¹, François Thil², Jane C. Wheeler³, Thomas Cucchi¹, Nicolas Goepfert⁴

¹AASPE-Archéozoologie, Archéobotanique: Sociétés, Pratiques et Environnements UMR 7209 : MNHN, CNRS - Paris, France.

²LSCE-Laboratoire des Sciences du Climat et de l'Environnement UMR 8212: CNRS, CEA, UVSQ - Gif-sur-Yvette, France.

³CONOPA-Instituto de Investigación y Desarrollo de Camélidos Sudamericanos, Av. Reusche M4, Pachacamac, Lima, Peru.

⁴ArchAm-Archéologie des Amériques UMR 8096: CNRS, Université Paris 1-Panthéon-Sorbonne – Paris, France.

*Corresponding author: **Manon Le Neün**: manon.le-neun@edu.mnhn.fr and **Nicolas Goepfert**: nicolas.goepfert@cnrs.fr.

Abstract:

The Andean highlands challenged but did not prevent human exploration and occupation starting in the Late Pleistocene. The timing and nature of these events is an ongoing area of research and debate for which reliable chronologies are required. Our goal is to revise the chronological framework of the Telarmachay rockshelter, a key site from the Andean highlands. To achieve this objective, we have conducted a new AMS dating programme utilizing 33 camelid bone samples from 6 archaeological layers and used a Bayesian modelling approach to determine the chrono-stratigraphy. Our chronology spans a greater than 5000 year sequence dated between 9.0-8.0 and 3.7-3.1 kyr BP, permitting reassessment of the antiquity and duration of the Telarmachay occupation, facilitating comparison with other sites, and allowing examination of domestic and symbolic practices in relation to Holocene climatic variation in the Central Andes. This study highlights the importance of the Junín area in the Andean highland occupation sequence. It also underlines the need for new radiocarbon dates to reassess previous data and directly date artifacts.

Keywords: Central Andes, Peru, Andean Prehistory, Holocene, Telarmachay, Radiocarbon AMS dating, South American Camelids.

Introduction

Determination of how and when the South American highlands were explored and colonized by humans is a subject of ongoing research and debate (Borrero and Santoro 2022). At an altitude of 3500-4500 meters above sea level, the puna is the highest ecosystem permanently inhabited by humans in the Andes (Tosi 1960; Dollfus 1978; Pulgar Vidal 1981; Olson *et al.* 2001; Aldenderfer 2006). This natural region extends from central Peru to central

Argentina and is composed of five ecoregions: the Central Andean dry puna, Central Andean puna, Central Andean wet puna, High Monte and the Southern Andean Steppe that includes Lake Titicaca, the largest lake in South America and one of the highest water surfaces on the planet (Troll 1968; Olson *et al.* 2001; Dinerstein *et al.* 2017). The puna is considered a harsh environment for human habitation due to low oxygen levels, high solar radiation, extreme temperature fluctuations and the high energetic cost of subsistence (Baker and Little 1976; Rademaker *et al.* 2014). Nonetheless, the harshness of the climate can be relative and perhaps should not be emphasized as a major factor effecting early human colonization (Capriles *et al.* 2016). The Andean highlands challenged, but did not prevent, human exploration and occupation starting in the Late Pleistocene (Dillehay 2014). The region provides a diversity of seasonally abundant food resources, as well as drinking water and siliceous rock for stone tool manufacture, that were available year around (Capriles *et al.* 2016; Rademaker and Moore 2019).

Recent research focused on the South-Central Andes has produced evidence of ancient hunter-gatherer occupation and the relationship between climate and nature of human occupation in southern Peru (Rademaker *et al.* 2014; Moore and Rademaker 2016; Chala-Aldana *et al.* 2017 Oct 27; Rademaker and Hodgins 2018; Karakostis *et al.* 2021; Meinekat *et al.* 2021), Northern Chile (Osorio *et al.* 2017), Bolivia (Capriles *et al.* 2016) and northwestern Argentina (Yacobaccio 2017)(Figure 1). Extensive work conducted by Rademaker and his team at Cuncaicha, in the high-altitude Pucuncho Basin, Peru, provides evidence of a coast-highland Paleoindian settlement system (Rademaker *et al.* 2014). Nevertheless, there is still debate as to whether or not these hunter-gatherers were year round residents occupying multiseasonal base camps, or if seasonal occupations were the norm (Capriles *et al.* 2016; Rademaker *et al.* 2016) in the Andean highlands at the end of the Pleistocene (Jodry and Santoro 2017). These recent studies, based on literature review and multidisciplinary

approaches comprising lithic, faunal and botanical analysis, as well as ^{14}C dating, have undoubtedly re-evaluated previous knowledge and preconceptions about early occupation of the highlands.

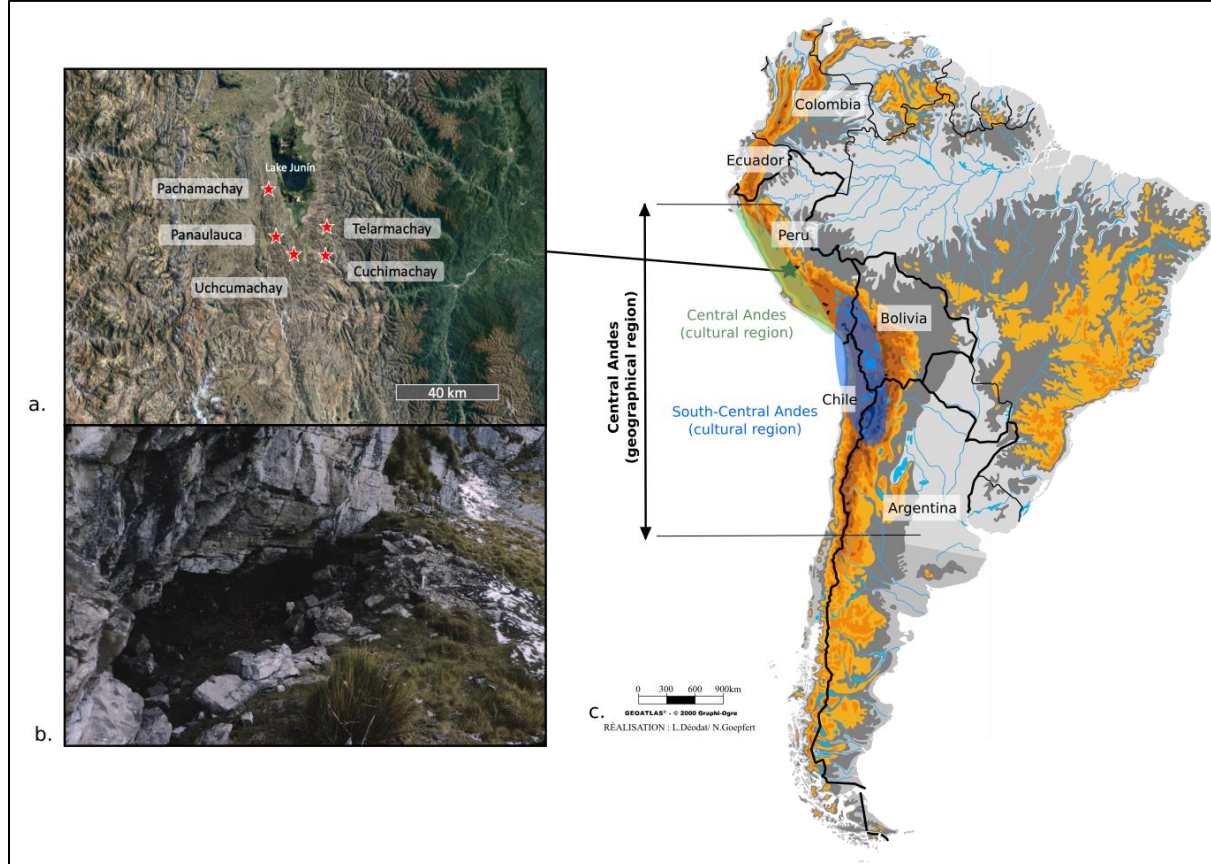


Figure 1: study area: a., location of the Puna of Junín archaeological sites discussed in the text, the map was modified from © Google Earth; b., view of the Telarmachay rockshelter entrance; c., location and delimitation of the Central and South-Central Andean cultural regions.

The Central Andes wet puna ecoregion was another major area of early settlement by human groups (Wheeler Pires-Ferreira *et al.* 1976; Lavallée *et al.* 1985; Rademaker and Moore 2019). The wet puna extends along the Andes of Peru and Bolivia with snow-capped peaks, mountain meadows, high lakes, plateaus and valley landscapes (Olson *et al.* 2001; Dinerstein *et al.* 2017). Apart from study of the Quishqui Punku site in Peru (Ortiz and Lynch 2016), current knowledge of the Central Andes is based mainly on pioneering studies carried out from

the 1950's to the 1990's in the puna and the lower elevation yunga natural region, at the sites (in geographic order north to south) of Guitarrero (Lynch *et al.* 1985), Kotosh (Wing 1972), Lauricocha (Cardich 1958; Cardich 1964; Wheeler Pires-Ferreira *et al.* 1976), Pachamachay (Wing 1975; Wheeler Pires-Ferreira *et al.* 1976; Rick 1980; Kent 1982), Panaulauca (Wheeler Pires-Ferreira *et al.* 1976, Moore 1989 ; Rick and Moore 1999), Uchcumachay (Wheeler Pires-Ferreira *et al.* 1976 ; Kaulicke 1980; Kaulicke 1999) and Tarma (Wing 1972). Compared to the South-Central Andes (Figure 1), the central part of Central Andes (Figure 1) has not benefited from new research, such as recent bioarchaeological analysis and ¹⁴C dating. One reason is the terrorist violence in Peru between the 1980s and 2000s that put an abrupt end to archaeological fieldwork at high-altitude until quite recently (Salcedo Camacho and Marcos 2019). Of particular interest is the Puna de Junín and the site of Telarmachay, a rockshelter located at an altitude of 4420 meters above sea level (11° 11' S latitude and 75° 52' W longitude) (Lavallée *et al.* 1985; Lavallée 1990) located 20 km from lake Junín (Figure 1). Telarmachay was excavated under the direction of Danièle Lavallée and Michèle Julien as part of the "Junín-Palcamayo" project between 1974 and 1980 (Lavallée *et al.* 1985; Lavallée 1990) and the faunal remains were studied by Jane Wheeler (1976, 1985, 1999). Excavation of the 35 m² surface and a depth of between 0.80 and 3 m of the site was performed by *decapage*, an unusual method for the Andes at the time, allowing a thorough analysis of the use of space in the shelter and the patterns of change through time. Lavallée and her team collected a large quantity of well-preserved material including nearly 37,000 lithic and 400,000 faunal remains. Faunal evidence suggested an *in situ* domestication process for the two wild South American camelid (SAC) species (Wheeler 1985, 1999). To date, it is the oldest known domestication center in the Andes (Lavallée *et al.* 1985; Wheeler 1985; Mengoni Goñalons and Yacobaccio 2006). Three human burials were also recovered which count among the scarce skeletal remains dating from the Preceramic period in the highlands (Julien *et al.* 1981; Lavallée *et al.* 1985; Santoro

et al. 2005; Fehren-Schmitz *et al.* 2015; Lindauer *et al.* 2015; Galván *et al.* 2016; Rademaker and Hodgins 2018; Haas *et al.* 2020; Nakatsuka *et al.* 2020). The stratigraphy of the site is composed of 6 layers classified from the oldest - layer VII - to the most recent - layer II - dated by radiocarbon and thermoluminescence (Pereyra Parra *et al.* 1982; Pereyra Parra *et al.* 1983; Lavallée *et al.* 1985; Lavallée 1990; Metcalf *et al.* 2016). Most of the ¹⁴C dates (29/33) were obtained before the advent of AMS and are therefore associated with large error bars (Appendix 1). Lavallée and colleagues rejected the anthropogenic nature of one Pleistocene charcoal date (Pucp-1825, 12 040 ± 120 BP) and described a sequence ranging between 9.0 to 2.0 kyr BP (Lavallée *et al.* 1985; Lavallée 1990) suggesting that the rockshelter and its surroundings exerted a strong attraction for human groups over 7000 years. Telarmachay thus offers the opportunity to document different aspects of domestic and symbolic life of the ancient human inhabitants and bring insight to the current debate about hunter-gatherer long-term residence at the site.

Understanding of the timing of major cultural events worldwide has improved thanks to advances in radiocarbon dating methods including AMS measurement, calibration and modelling using Bayesian statistics (Bronk Ramsey 2009a). These results make clear the importance of obtaining new dates in order to improve the chronostratigraphies of previously excavated sites. Indeed, the old dating systems affected by sampling problems and measurement accuracy or lack of calibration, make it impossible to relate major culture change events, identify transitional behaviours, or determine dispersal patterns linked to human activities (Higham *et al.* 2011). For the Andes, comparative syntheses of Peruvian coastal and high altitude sites (Rademaker *et al.* 2013 Appendices A and B; Salcedo Camacho and Marcos 2019), with sites in the central altiplano of Bolivia (Marsh 2015) and northern Chile and Argentina (Rademaker *et al.* 2018) demonstrate the need for new calibration of published dates. Chronostratigraphies have traditionally been based on analysis of charcoal samples, but new

techniques utilizing human and animal bone samples have, for example, made it possible to date the domestication of different animals worldwide (Brunson *et al.* 2020; Cromb   *et al.* 2020), and date bones with cut marks and human produced modifications from Early Upper Palaeolithic sites in Europe (Higham *et al.* 2011). Direct dating of human and camelid bone remains from early high altitude sites in Peru (Fehren-Schmitz *et al.* 2015; Lindauer *et al.* 2015; Rademaker and Hodgins 2018) also demonstrates the importance of reevaluating chronological sequences, based on charcoal samples or accompanying artifacts, in order to improve the understanding of symbolic, domestic and strategic human practices.

Dating of the Telarmachay layers by Lavall  e *et al.* (1985) was performed prior the advent of AMS and thus typically had an error of 100 years or greater resulting in errors bar on an order of half a millennium after calibration (Appendix 1). Our evaluation of these dates with the “SHcal20” curve Hogg *et al.* (2020) suggest that occupation could have begun as early as 14 kyr BP (Figure 2 - in blue). But this early date is based on one single charcoal which was rejected by Lavall  e *et al.* (1985). Dates for the rest of the occupation range between 10-8 kyr BP to the beginning of our era. However, three samples of layer VI do not fall within their anticipated age range (Figure 2- in red). Calibration of the former corpus of dates, based on charcoal samples and four SAC bones (Metcalf *et al.* 2016), reveals shifts in layer boundary dates (Appendix 1 and Figure 2). Thus, there is a strong probability that the chronology of the site was biased and Telarmachay chronostratigraphy should be used cautiously.

The main goal of the present paper is to revise and re-evaluate the chronological framework of Telarmachay. To achieve this objective, we calibrated the previous charcoal dates and conducted a new AMS dating programme utilizing camelid bone samples from six layers, VII to II, at the site. The new chronological framework permits discussion of the antiquity and duration of the Telarmachay occupation, and the evolution of human domestic

and symbolic practices, the SAC domestication process, and human inhumation at the site, in relation to climatic variation during the Holocene.

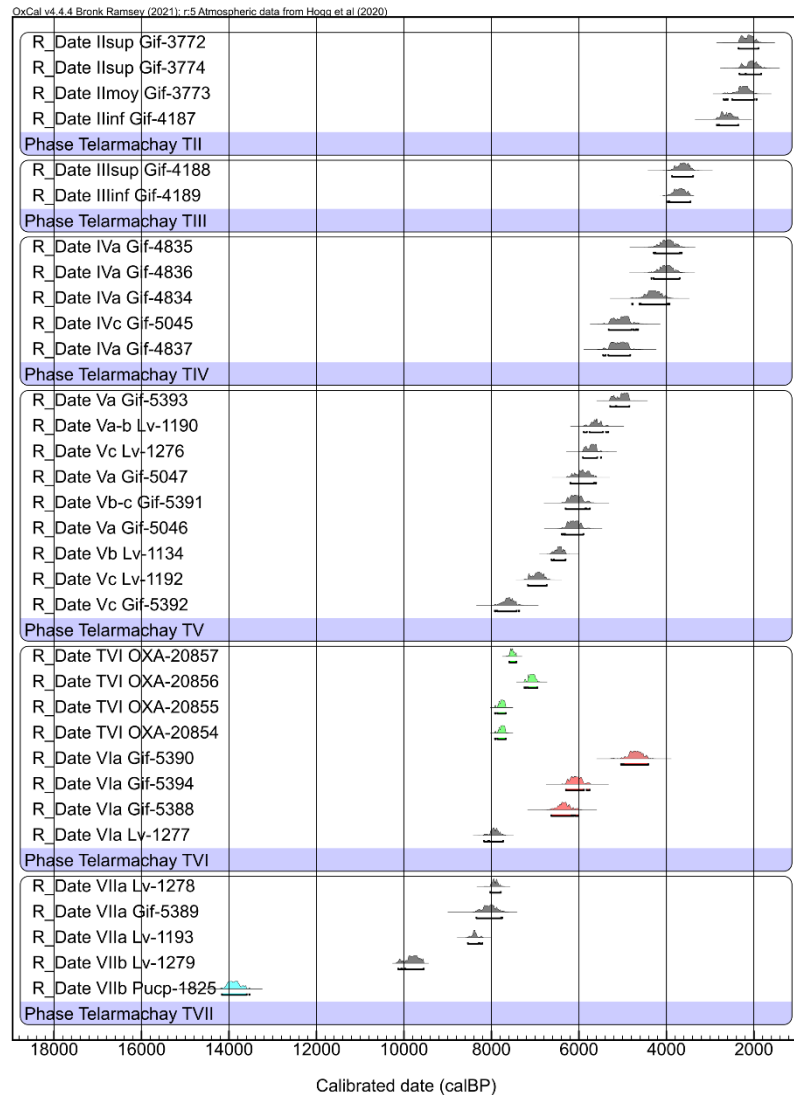


Figure 2: calibrated intervals (BP) from the charcoal dates obtained in the 1980s (Lavallée and Julien 1980; Lavallée et al. 1985) with the “SHcal20” curve (Hogg et al. 2020). The layer VII boundary start is in blue, the three displaced layer VI samples are in red and the four SAC bones dated by Metcalf et al. (2016) are in green.

Material and Methods

Selection of camelid bones

The archaeological dataset is composed of 39 samples including 26 talus, 7 mandibles, 2 phalanges, 1 calcaneus and 3 undetermined bones. Spatialization and archaeological structures were taken into account in order to homogenize the selection of samples. The distribution per layer is the following: VII: n = 4; VI: n = 10; V: n = 7; IV: n = 10; III: n= 4 and II: n = 3 (Appendix 2).

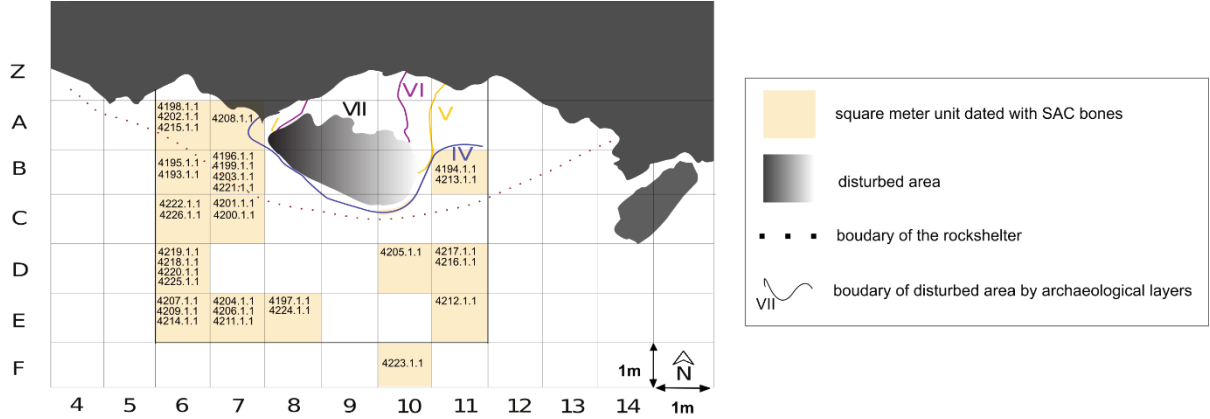


Figure 3: Telarmachay rockshelter excavation plan based on Lavallée et al. (1985) which reports the excavation directed by Danièle Lavallée and Michèle Julien between 1974 and 1980. A disturbed area was identified under the rockshelter (grey gradient) and the boundaries for each layer are represented by black for the Layer VII, purple for layer VI, yellow for layer V and blue for layer IV). Numbers (“ECHo”) refer to radiocarbon dates performed using the compact AMS ECHoMICADAS and the SAC bone samples selected for this study. Their location is indicated on the excavation plan by the (yellow) squares.

Preparation of samples and collagen extraction

The bones were mechanically cleaned by abrasion using a tungsten drill tool. They were then cut into 1 gr subsamples and ground to powder, sieved to separate the 350-700 µm grains from which 150 mgs were used for collagen extraction, following Zazzo *et al.* (2019). The bone was demineralised in a 1M HCl solution for 20 min at room temperature. Due to the good

preservation of the Telarmachay material, two 10 min treatments in NaOH (0.125M) were sufficient to remove any humic and fulvic acids. The samples were then solubilised in a 0.01M HCl solution for 17 h at 95°C and filtered. Finally, the gelatin samples were freeze-dried for 48 h and the collagen yield (%coll), expressed as the mass of collagen obtained per mass of processed bone sample, was calculated. Bone preparation and collagen extraction were performed in the *Plateau de sclérochronologie* (UMR7209, CNRS/MNHN,) and the laboratory of *Cosmochimie de l'Institut de minéralogie, de physique des matériaux et de cosmochimie* (IMPMC, UMR 7590 – Sorbonne Université, CNRS/MNHN/IRD) in Paris.

Combustion, graphitization and radiocarbon measurement

2.5 mg of bone collagen from each sample were wrapped in an ultra-light tin capsule and combusted in an Elemental Analyser (EA) and then transferred to an AGE 3 automated compact graphitisation system. Two oxalic acid II standards and two phthalic anhydride blanks were treated with the unknowns for every 10 samples. The reduction was carried out in seven quartz reactors, each containing 5 mg of iron catalyst. Prior to burning each sample, an aliquot of that sample was burnt to minimise cross-contamination. Following combustion, %C and %N, as well as C/N atomic ratios of each individual sample were calculated. Only samples which met the three following quality control criteria were then pressed into targets and dated. The state of collagen preservation was assessed using the following criteria: (1) collagen yield (% coll), (2) percentage of carbon (%C) and nitrogen (%N) in collagen (Ambrose 1990) and (3) measurement of C/N atomic ratio (DeNiro 1985). For the collagen yield (%coll), samples with a higher than the cut-off value of 1 per cent are necessary and used by radiocarbon labs (Van Klinken 1999; Brock *et al.* 2010). The abundance of carbon and nitrogen in modern bones ranges from 13-47% and 4.8-17.3% respectively (Ambrose 1990), extraction residues containing less than 8% carbon and 3% nitrogen are then chemically and isotopically altered

(Oberlin and Valladas 2015). The C/N atomic ratio of unweathered bone collagen classically ranges from 2.9 to 3.6. A recent study has shown that the criteria for controlling collagen purity may be stricter for bones found in subsurface contexts or at mid-latitudes (Zazzo *et al.* 2019). The authors highlighted that collagen samples with C/N ratios outside the range of 3.1 to 3.3 or without at least 5% extraction efficiencies should be considered altered or contaminated and of unreliable dating.

The graphite targets were analyzed using the compact AMS ECHoMICADAS in the *Laboratoire des Sciences du Climat et de l'Environnement* (LSCE, UMR 8212, CNRS/CEA/UVSQ) in Saclay (France). Data reduction was performed using BATS software (version 4.07). Radiocarbon dates were calibrated using the latest Southern Hemisphere curve (SHcal20) (Hogg *et al.* 2020), the mixed curve IntCal20 (Reimer *et al.* 2020) and SHcal20 (Hogg *et al.* 2020) approach (Buck 2004; Ogburn 2012; Marsh *et al.* 2017; Marsh *et al.* 2018) and the latest version of Oxcal software (v4.4) (Bronk Ramsey 2009a; Ramsey and Lee 2013).

Statistical analysis: Bayesian Modeling

A Bayesian modelling framework has been developed to analyze the corpus of radiocarbon dates. This approach allows stratigraphic information and radiocarbon age probabilities to be incorporated into a statistical model (Bronk Ramsey 2009b). The OxCal software uses a Markov Chain Monte Carlo (MCMC) method to successively sample solutions of Bayes' theorem, which is the basis of the Bayesian approach. The model data represents the radiocarbon measurements, or "likelihoods". The a priori laws in the model are composed of information on the relative previous sequences known a priori with the meticulous excavations realized by Danièle Lavallée and her team. We know, for example, that layer V is younger than layer VI, and we are able to use this order information statistically. The data are transformed using the calibration curve to form a new posterior distribution, called the posterior distribution.

The internal consistency of the posterior distributions of the model can be tested using fit indices. Posterior distributions that appear reasonable produce high agreement indices, while those that appear to differ produce lower indices, leading us to question their position or reliability.

The model (v0) that we have developed consists of a series of six phases, represented by the successive excavation layers or strata, and the boundaries between them (Appendix 6-c). Due to the smaller number of dates in Phases III ($n = 4$) and II ($n = 3$), these have been grouped into a single Phase “III-II”. We included all dates made on the bones in this study as well as the four camelid bone dates from the Oxford laboratory and published by Metcalf *et al.* (2016). We tried to include the charcoal dates but it caused the model to fail. This was probably due to the large number of outliers and measurement uncertainties attached to these measurements. Therefore, the model only contains the most recent bone for which the origin and radiocarbon measurement is controlled by us. Dates were entered into Oxcal software. As the differences in age per layer exceeded the uncertainty in ages, we sequenced these phases by postulating a discontinuous phasing (with period of abandonment) between the six different layers of the Telarmachay occupation. Each layer is thus separated by two boundaries (beginning and end)(Appendix 6-c).

Results

New Radiocarbon dating of the camelid bones

Of the 39 skeletal elements sampled, 36 contained collagen and 33 of these were selected for AMS ^{14}C dating (Appendix 2). Well-preserved collagen with yields ranging from 7.3% to 25.3% was obtained from the 33 samples. The C/N values vary between 3.19 and 3.25 indicating an absence of soil carbon contamination (Appendix 2). The reliability of raw

radiocarbon ages from these bones is therefore excellent, placing the site occupation between $7\,860 \pm 30$ and $3\,420 \pm 25$ BP. Calibration with the latest Southern Hemisphere curve (SHcal20; Hogg *et al.* 2020; Appendix 6-b) provides an occupation ranging from 8.7-8.5 and 3.8-3.5 kyr BP (Appendix 2). We also tested the mixed calibration curve IntCal20 (Reimer *et al.* 2020) and SHcal20 (Hogg *et al.* 2020) approach (Buck 2004; Ogburn 2012; Marsh *et al.* 2017; Marsh *et al.* 2018; Appendix 6-e and f). This test provides a very slight difference (Appendix 4-a and b), so we retained the latest Southern Hemisphere curve for the Bayesian model.

Bayesian modelling

The results obtained with the first Bayesian model (Appendix 6-c) do not converge and the *a priori* proposed scheme is therefore not validated. This is most certainly related to the fact that some bone samples are not in place in the stratigraphy. Given that all the measurements have been validated from a physico-chemical point of view, there is not sufficient cause to reject the dates manually. For this reason, we created a second Bayesian model (Appendix 6-d) incorporating the possibility that each bone has a 5% probability to be an outlier within the overall model. We add a symmetric 't' outlier density, based on the age of the sample, which is used as a statistical weighting criterion in the modelling (Bronk Ramsey 2009b)(Appendix 4-b). Our model identifies 14 samples with a probability of more than 5% of being outliers and 8 samples with a probability of more than 20 % (Appendix 3). Moreover, the convergence of the dates resulting from this second model also suggests grouping layers III and II dates into a single set (Table 1). We now provide a new chronostratigraphy with specified boundaries that covers a period between 9.0-8.0 and 3.7-3.1 kyr BP (Figure 4).

Layer number (BP)	Boundary start		Boundary end	
III-II	5095	4433	3682	3119
IV	6605	5938	5849	4507
V	7067	6743	6650	6046
VI	7885	7720	7141	6887
VII	9016	8035	7934	7734

Table 1: new start and end boundaries for the Telarmachay layers from the Bayesian age model using a t-type outlier model method with prior probabilities set at 0.05. The model is based on camelid radiocarbon ages and calibrated using the (SHcal20) curve (Hogg et al. 2020).

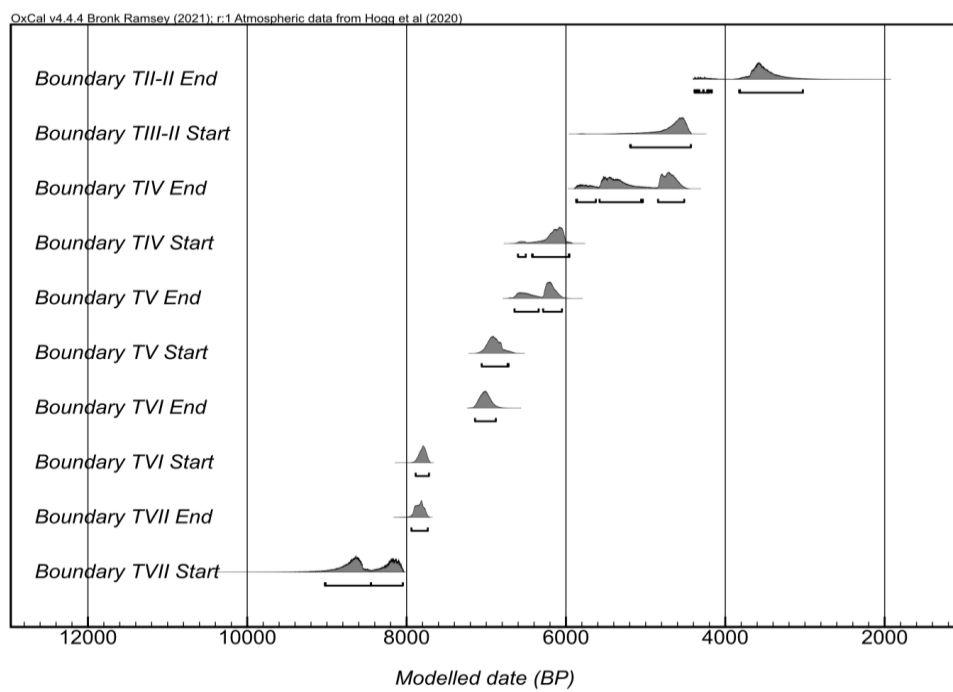


Figure 4: Start and end boundaries for the Telarmachay rockshelter layers from the Bayesian age model using a t-type outlier model method with prior probabilities set at 0.05 using Oxcal. The radiocarbon ages are calibrated using the (SHcal20) curve (Hogg et al. 2020).

The dark outlines represent the posterior probability distributions (i.e., the results after the Bayesian modelling).

Differences between the two types of chronology at Telarmachay

Lavallée *et al.* (1985) proposed a continuous occupation of Telarmachay without significant abandonment during 7 millennia between 9.0 and 2.0 kyr BP. They claimed that the chronology was consistent despite 7 charcoal samples collected within the hearths of layers V and IV that were significantly younger than the rest of the samples. The analysis of sediment deposits indicated a hiatus between the end of layer VI and the beginning of layer V that is not reflected by the radiocarbon dates. Its duration would not have exceeded one or two centuries (Lavallée *et al.* 1985). Thermoluminescence dating of sherds from the two last layers of the chronology (III and II) suggested an earlier end boundary for the occupation around ca 3.2 and 2.1 kyr BP (dates provided by the authors: 1260 and 160 BCE; Pereyra Parra *et al.* 1982; Pereyra Parra *et al.* 1983). Our calibration of charcoal dates with the last curve of the southern hemisphere draws a different picture and shifts the layer boundaries as the occupation began around 14.2-13.5 kyr BP and ended around 2.3 and 1.8 kyr BP (Appendix 1 and 7 and Figure 2). Three charcoals from layer VI are too recent and therefore not in place (Figure 2 - in red). We interpret these shifts as the result of possible movement in the stratigraphy. Our chronological frame based on the modelled radiocarbon age from camelid bones provides an occupation reduced to a 4 millennia period ranging between 9.0-8.0 and 3.7-3.1 kyr BP (Table 1, Figure 4 and Appendix 7). The main discrepancy in chronologies concerns layers III and II and questions the cultural attribution of the last occupation of the rockshelter (Appendix 7). Different cultural chronologies are used in the Andes, even for the same cultural zone (Conlee and Ogburn 2004). Depending on the chronological classification system used and the date retained for the end of the layer, the final Telarmachay occupation corresponds to various

named periods. According to our bone dates the Telarmachay occupation ended during the Late Preceramic Period/Initial Period or Archaic/Formative Period. According to calibrated charcoal dates Telarmachay occupation ended during the Late Preceramic Period/Initial Period/Early Horizon/Early Intermediate Period, or the Formative Period (Figure 5).

Discussion

Early occupation at the end of the Pleistocene?

Recent research concerning the antiquity of early hunter-gatherer settlements in the Andean highlands has generated much discussion. Firm evidence now places the initial occupation of the highlands to 13,000 cal BP and the start of more intensive occupations around 10,000 years ago, followed by later regional variations (Albarracín-Jordan and Capriles 2011; Capriles and Albarracín-Jordan 2013; Rademaker *et al.* 2014; Capriles *et al.* 2016; Jodry and Santoro 2017; Loyola *et al.* 2017; Osorio *et al.* 2017). Calibration of the ¹⁴C dates from a single charcoal sample from Telarmachay provides an age between 14.2-13.5 kyr BP (Pucp-1825, Appendix 1 and Figure 2), suggesting that Telarmachay could have been occupied from the Late Pleistocene on. It is noteworthy that our sequence established from the camelid bones does not support anthropic activities preceding 9.0 kyr BP. Lavallée *et al.* (1985) initially rejected the anthropogenic nature of this charcoal sample arguing the Puna of Junín had probably not yet been released from the glaciers at that time. Climatic knowledge has progressed since the eighties, and sediment analysis of Lake Junín now shows that deglaciation began as early as 22.5 kyr BP (Woods *et al.* 2020). Stable isotope and lake level records of three proglacial lakes located between 9 and 10°S in the Peruvian Andes (Cordillera Blanca, Cordillera Huayhuash and Cordillera Raura) show that 12.0 and 8.0 kyr BP was a period of reduced glacial extent, marked by decreasing humidity with the arrival of arid and warm conditions (Stansell *et al.*

2013). Moreover, Rademaker *et al.* (2014) found that the Pucuncho Basin glaciers did not represent a barrier to human migration and settlement during the Pleistocene. An AMS radiocarbon date of 22.220 ± 130 BP from a metacarpal of *Vicugna* sp. recovered in the Cueva Rosello site, Puna of Junín, provided a calibrated age of 26.6–26.9 kyr BP (Shockey *et al.* 2009). If the authors mentioned that ungulate remains from this site were carried into the cave by predators, the *Vicugna* sp. remain suggests that camelids also migrated into the puna ecosystem in Junín at least since the end of the Pleistocene (Shockey *et al.* 2009). It is therefore likely that the area around Telarmachay was habitable by 22.5 kyr BP and particularly from 12.0 kyr BP. Calibration of the ^{14}C dates available from the literature for 4 additional Junín sites indicates that the site of Pachamachay may also have been occupied at the end of the Pleistocene and that all the sites may also have been occupied over long periods (Figure 5; **Appendix 5**).

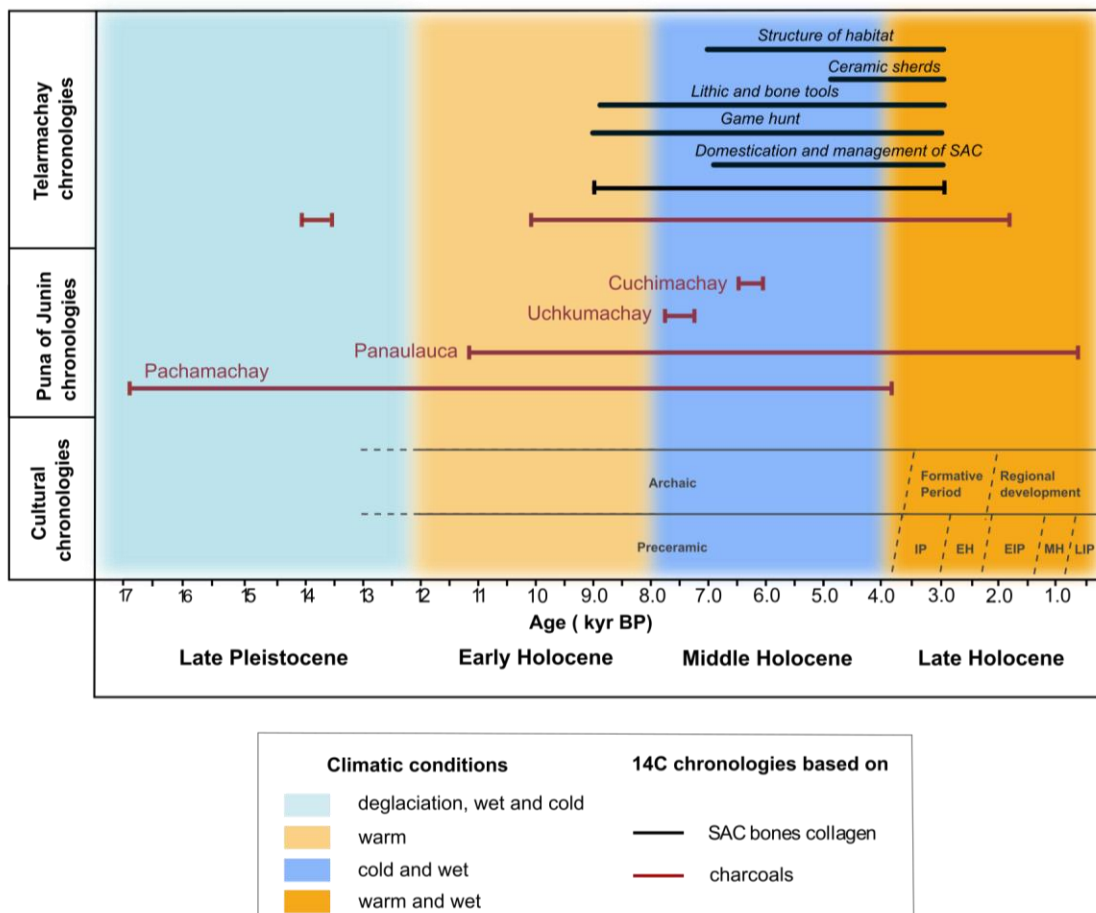


Figure 5 : Comparison of climate change, occupation chronologies at five major sites from the Puna of Junín (Peru, Central Andes) and cultural chronologies for the Central Andes: Archaic ca. 12-3.5 kyr BP (Vaughn 2006); Preceramic ca. 11.5-6.75 kyr BP; Late Preceramic ca. 6.75-3.8 kyr BP; Formative Period ca. 3.5-2.5 kyr BP; IP Initial Period ca. 3.8-2.85 kyr BP; EH Early Horizon: ca. 2.85-2.2 kyr BP; EIP Early Intermediate Period ca. 2.2-1.5 kyr BP; MH Middle Horizon ca. 1.5-1.35 kyr BP; LIP Late Intermediate Period ca. 1.35-0.48 kyr BP (Keatinge 1988; Conlee and Ogburn 2004). General climatic conditions, aridity and temperature are indicated by different colours based on data from (Seltzer et al. 2002; Bird et al. 2011; Stansell et al. 2013; Woods et al. 2020). The two chronologies represented for Telarmachay were established from the calibration of 33 ^{14}C dates on SAC bone collagen (brown) and the calibration of ^{14}C charcoal dates (black) from Lavallée et al. (1995), Lavallée (1990). The main human activity chronologies at Telarmachay (brown) are based on Lavallée et al. (1985) and compared to the SAC bone collagen chronology. Chronologies of other Junín sites are determined by the calibration of ^{14}C dates available from the literature: Pachamachay (Rick 1980; Rademaker and Moore 2019), Panaulauca (Moore 1998; Rick and Moore 1999; Rademaker and Moore 2019; Salcedo Camacho and Marcos 2019), Uchkumachay (Kaulicke 1999; Salcedo Camacho and Marcos 2019) and Cuchimachay (Salcedo Camacho and Marcos 2019; Appendix 5).

Holocene occupation

Our ^{14}C data confirm the attractiveness of Telarmachay rockshelter with long occupation by human groups encompassing the Early to Late Holocene. Throughout the occupation of the site there is continuity in the tools used for exploitation of animals, the main subsistence resource (Julien et al. 1987). These include stone tools (knives, scrapers and bifacial points) as well as bone tools used for hide processing (*queursoirs*, burnisher, punches)

or stone working (billet and pressure tool) (Julien *et al.* 1987). Tools used for stone working are limited, while the majority of tools (88.74%) seem to be related to processing of animals after hunting and for work on soft materials such as skins. Thus, the rockshelter was not only a place reserved for primary exploitation of large herbivores (butchery, consumption) but also for the transformation and manufacturing work directly related to raw animal matter (Lavallée *et al.* 1985).

According to Lavallée *et al.* (1985), an intensification in use of the rockshelter occurred through time corresponding to the deposition of layers VII to VI. At first, during the Late Holocene, a small area of habitation was available under the rockshelter and a low density of remains were found. However, the homogeneity of the deposits without abandonment and zooarchaeological remains suggested that the site was regularly used as a simple short hunting camp (Layer VII, now dated between 9.0 - 8.0 and 7.9 - 7.7 kyr BP (Table 1, figure 4). In the 1985 publication the limited faunal sample analyzed from this layer made it impossible to determine the season of occupation (Lavallée *et al.* 1985). Subsequent archaeozoological analysis found that young camelids (under one month) represented about 30 % of the total SAC remains, suggesting a seasonal occupation between November and March (Wheeler 1985; Wheeler 1999). Gradual intensification of rockshelter occupation is indicated by an increase in the density of tool remains in Layer VI (now dated between 7.9-7.7 and 7.1-6.9 kyr BP (Table 1, figure 4) and corresponds to the transition to the middle Holocene. Despite the large number of tools, stone working was limited and the tools were most likely made elsewhere (Lavallée *et al.* 1985). Our dating provides a maximum age (or *terminus post quem*) for human remains found in layer VI now dated be between 7.9-7.7 and 7.1-6.9 kyr BP. The burials of two women and a child indicates the existence of funerary practices at the rockshelter (Julien *et al.* 1981). They represent rare evidence of symbolic practices of the ancient puna hunter-gatherers and

may reflect, subject to a new study of the burials and their associated material, the female participation in highland activities such as big-game hunting (Haas *et al.* 2020).

Layer V, now dated between 7.1-6.8 and 6.6-6.0 kyr BP (Table 1, figure 4), witnesses new steps in use of the rockshelter. First, the foundations of a true habitation structure are found at the entrance of the shelter, extending the small naturally covered area to a larger living area protected from the weather by a wall of stone blocks. The enlarged living area may indicate more frequent, regular and longer, possibly seasonal, occupation periods (Lavallée *et al.* 1985). This enlarged domestic interior space was not maintained in layer IV, formerly dated between 5 and 3.8 kyr BP and now corresponds to 6.4-6.0 and 5.8-4.5 kyr BP (Table 1, figure 4). Instead, aligned blocks that may represent a low wall separating the interior and exterior of the shelter, defining a small living space and possibly reflecting a smaller population than during Layer V. This period also saw the emergence of a new mode of animal resource management based on the use of domestic camelids even though game hunting persisted (Wheeler 1985). The diachronic study of camelid bones uncovered the early domestication of the alpaca and llama (Wheeler 1985) previously dated between 6.0 and 5.5 BP and 5.0 to 3.8 kyr BP, respectively, and now between 7.1-6.8 and 6.6-6.0 kyr BP and between 6.4-6.0 and 5.8-4.5 kyr BP, respectively. The new chronology confirms the antiquity of alpaca domestication in the Puna of Junín and its precedence compared to other early occurrences identified between 3.5 and 2.4 kyr BP in the Southern Central Andes (Díaz-Maroto *et al.* 2021). Llama domestication in Junín falls between that reported at centers located to the south that are dated around 7.1 kyr BP and 4.4 kyr BP (Mengoni Goñalons and Yacobaccio 2006; Cartajena *et al.* 2007; Mengoni Goñalons 2008; Cartajena 2013). During layer IV occupation, llama and alpaca herding and butchery activities may have occupied most of the time of the Telarmachay occupants (Lavallée *et al.* 1985).

The early to mid-Holocene period is characterized by important climatic changes (Stansell *et al.* 2013) that may have influenced the occupation of Telarmachay. The Early Holocene is marked by arid and warm conditions (Stansell *et al.* 2013) with a significant reduction of the South American Monsoon (SASM)(Bird *et al.* 2011). Despite this long-term dry period, the presence of hunter-gatherers at Telarmachay suggests that the habitats surrounding the rock shelter were attractive. This is consistent with human presence elsewhere in the Andean highlands and the absence of hyper-arid conditions following the more humid Late Pleistocene phases (Jodry and Santoro 2017). Utilization of the rockshelter increased with the onset of colder and wetter conditions during the Middle Holocene (Stansell *et al.* 2013). Intensification of human occupation through the end of the Early Holocene and during the Middle Holocene is consistent with Rademaker and Moore's data (2019) which showed that after 9000 BP, the best-watered habitats were situated in the wet puna of the Central Andes. Panaulauca and Pachamachay rockshelter in the Puna of Junín were continuously occupied and increasingly used through the Middle Holocene as indicated by the volume of cultural material such as the count of formal chipped-stone tools and the weight of chipped-stone debitage and faunal remains (Rademaker and Moore 2019). In comparison, the dry puna of the South-Central Andes became drier (Rademaker and Moore 2019) and occupation density at the sites of Hakenasa (northern Chile) and Hornillos-2 (northwestern Argentina) decreased (Rademaker and Moore 2019). The influence of Early to Mid-Holocene climatic change was not recognized in the original Telarmachay studies due to the limitations of dating technology prior to the establishment of ¹⁴C calibration curves and the scarcity of climatic studies at the time.

Layers III and II, previously dated between 3.8-2.8 kyr BP and 2.8-2.0 kyr BP, now date between 5.2-4.4 and 3.7-3.1 kyr BP (Table 1, figure 4). This occupation corresponds to the end of the Middle Holocene, a period of glacial resurgence and abrupt drop in temperature around 5 kyr BP (Stansell *et al.* 2013), and is followed by the onset of warm and wet climatic

conditions with glacial retreat from 4 kyr BP at the Middle to Late Holocene transition. The apparent reduction of rockshelter interior living space (still delimited by blocks), a decrease in the quantity of bone remains and an apparent shift in animal procurement strategy suggests changes in the timing and duration of occupation. A smaller population may have occupied the site, and year-round presence of llama and alpaca herders is suggested by the reduced frequency of very young camelids (born during the rainy season) and the increase in hunted animal remains (deer). The presence of numerous lithic scrapers, bone needles and punches, knives made of SAC scapulae, and a bone spindle-whorls indicate SAC fiber exploitation and spinning (Lavallée and Julien 1980). It is thought that the rockshelter was no longer used seasonally but was occupied year round by a very small number of people caring for domestic camelid herds (Lavallée 1988). Rick and Moore (1999) also observed decreased occupation density at Panalaucá during the late occupation based on faunal and lithic evidence (Rick and Moore 1999).

The changes in social organization that occurred in the Puna de Junín at the end of the Middle Holocene and during the transition to the Late Holocene have also been reported in other regions of the highlands (Keatinge 1988; Lavallée 1995). Aldenderfer (2004) considered that different areas of the Peruvian highlands Puna of Junín, Ayacucho Basin, the upper Osmore (Asana) drainage in Moquegua, Chila and Ilave drainages in the Lake Titicaca Basin and the Central Andean high sierra with the famous sites of Huaricoto, Kotosh, La Galgada and Piruru, were occupied by potential “leaders”. These leaders experimented with different leadership strategies and had varying degrees of success in the development of their personal prestige through the use of lineage, ritual, and possibly small-scale warfare and conflict (Aldenderfer 2004). However, Aldenderfer (2004) claims that there was no emergence of obvious persistent leadership in the Puna of Junín during the Late Preceramic Period. If small populations of possibly sedentary llama and alpaca herders were present, there was no emergence of inequality

(Aldenderfer 2004). In adjacent mountainous regions the sedentarization of the population marks the beginning of monumental architecture (such as Kotosh, Piruru or La Galgada) with the advent of a ruling class (Keatinge 1988; Lavallée 1995). The north-central coast saw the florescence and the development of early complex centralized political systems such as the Casma valley (Pozorski and Pozorski 2008). For instance, research in the small valleys of *the Norte Chico* region has revealed a pattern of more than 20 large sites (Caral, Chupacigarro, Era de Pando, Pueblo Nuevo, Lurihuasi, Allpacoto among others in the Supe valley) with major residential and ceremonial centers dated between 5 and 3.8 kyr BP (on the base of 3000 and 1800 B.C. proposed in Haas *et al.* 2004). Although there is no evidence of change in social organization at Telarmachay, changes in pastoral activities may be related to these overall economic and social changes experienced by Pre-Hispanic societies. However, the discrepancies observed between the chronologies of the last layers (III and II) make it difficult to compare precisely cultural phenomena among sites within an ecological zone or from different ecological zones. This issue is particularly stressed for discussing the introduction of ceramics in highlands, as compared to other Andean regions. The introduction of pottery is an important event in the emergence of Andean civilisation (Kanezaki *et al.* 2021). The ceramics found at Telarmachay are have been directly dated by thermoluminescence to ca 3.2 and 2.1 kyr BP (Pereyra Parra *et al.* 1982; Pereyra Parra *et al.* 1983). According to a recent study, early evidence of pottery in the Central Andes is found between 4 and 3 kyr BP (Kanezaki *et al.* 2021), in keeping with 14C dating of these layers

Conclusion

This study provides new boundary models of the start and end dates of the archaeological layers of the key site of Telarmachay. Our chronology spans a greater than 4000

year sequence dated between 9.0-8.0 and 3.7-3.1 kyr BP. We compare this new sequence with previously established chronologies obtained through ^{14}C dates on charcoals at Telarmachay, Panaulaaca, Pachamachay, Uchkumachay and Cuchimachay to assess the antiquity and duration of the Telarmachay occupation, changes in the intensity of human occupation, subsistence practices and hunter-gatherer lifestyle, including the evolution of domestic and symbolic human strategies and practices in the Junín region as related to Holocene climatic variation. New dates and the reassessment of previous dates show that while the Andean highlands challenged human occupation it did not prevent human exploration and exploitation since the Late Pleistocene (Dillehay 2014). The Junín region was favorable to early human occupation thanks to a diversity of seasonally abundant food resources, with drinking water and siliceous rocks for stone tool manufacture available year around (Capriles *et al.* 2016; Rademaker and Moore 2019).

This study highlights the necessity of utilizing chronologies that make it easy to compare sites across the Central Andes. Furthermore, it also emphasizes the need for direct dating of artifacts that are linked to the cultural and social events and evolution under study. In this sense, the direct dating of SAC bones can provide a time frame to further explore the emergence of SAC domestication at the transition between Late Holocene to Middle Holocene and the subsequent economic development based on husbandry. Similarly, we provide a maximum age (or *terminus post quem*) for human remains at Telarmachay, but direct dating should be done to confirm their antiquity, as they are a rare witness of the funerary practices and symbolic activities of ancient highland hunter-gatherers. Finally, the transition to the Late Holocene saw another major step with the appearance of ceramics, although this requires further documentation with direct dating of sherds.

Acknowledgements:

We want to thank Torben Rick and Amanda Lawrence for access to the Telarmachay materials from the Bioarchaeological collection of the Smithsonian Institution and the Natural History Museum and their help during a mission by Manon Le Neün at the Smithsonian. We also thank Sonia Guillén (Centro Mallqui, Peru) and Denise Pozzi-Escot (Museo de Sitio Pachacamac, Peru) for their invaluable administrative assistance. Melinda Zeder (SI- NHM, USA) and Katherine Moore (University of Pennsylvania Museum, USA) are warmly thanked for their help and useful advice to address the huge Telarmachay collection. Danièle Lavallée and Michelle Julien provided invaluable information on the excavation of Telarmachay that they led in the puna during the years 1970 and 1980 and are also warmly thanked. This study was supported by the Région Île-de-France and the Domaine d’Intérêt Majeur “Matériaux anciens et patrimoniaux” (DIM-MAP, AAP 2018-3, project CAMELIDOM), the Action Transversale du Muséum (ATM CHRONOCAM) and Ecole Doctorale 227 “Sciences de la nature et de l’Homme: évolution et écologie” of the Muséum national d’Histoire naturelle and Sorbonne Université (ED227 MNHN-SU, France) and ANR CAMELANDES (ANR-15-CE27-0002-01) supervised by Nicolas Goepfert and Élise Dufour.

References

- Albarracin-Jordan J, Capriles JM. 2011. The Paleoamerican occupation of Cueva Bautista: Late Pleistocene human evidence from the Bolivian highlands. Current Research in the Pleistocene. 28(9).
- Aldenderfer M. 2004. Preludes to power in the highland Late Preceramic Period. Archeological Papers of the American Anthropological Association. 14(1):13–35.

Aldenderfer M. 2006. Modelling plateau peoples: The early human use of the world's high plateaux. *warch.* 38:357. doi:10.1080/00438240600813285.

Ambrose SH. 1990. Preparation and characterization of bone and tooth collagen for isotopic analysis. *Journal of archaeological science.* 17(4):431–451.

Baker PT, Little MA. 1976. Man in the Andes; a multidisciplinary study of high-altitude Quechua.

Bird BW, Abbott MB, Rodbell DT, Vuille M. 2011. Holocene tropical South American hydroclimate revealed from a decadally resolved lake sediment $\delta^{18}\text{O}$ record. *Earth and Planetary Science Letters.* 310(3–4):192–202.

Borrero LA, Santoro CM. 2022. Metapopulation Processes in the Long-Term Colonization of the Andean Highlands in South America. *Journal of World Prehistory.* 35(2):135–162.

Brock F, Higham T, Ramsey CB. 2010. Pre-screening techniques for identification of samples suitable for radiocarbon dating of poorly preserved bones. *Journal of archaeological science.* 37(4):855–865.

Bronk Ramsey C. 2009a. Bayesian analysis of radiocarbon dates. *Radiocarbon.* 51(1):337–360.

Bronk Ramsey C. 2009b. Dealing with outliers and offsets in radiocarbon dating. *Radiocarbon.* 51(3):1023–1045.

Brunson K, Lele R, Xin Z, Xiaoling D, Hui W, Jing Z, Flad R. 2020. Zooarchaeology, ancient mtDNA, and radiocarbon dating provide new evidence for the emergence of domestic cattle and caprines in the Tao River Valley of Gansu Province, northwest China. *Journal of Archaeological Science: Reports.* 31:102262. doi:10.1016/j.jasrep.2020.102262.

Buck CE. 2004. Bayesian chronological data interpretation: where now? Tools for constructing chronologies: crossing disciplinary boundaries.:1–24.

Capriles JM, Albarracin-Jordan J. 2013. The earliest human occupations in Bolivia: A review of the archaeological evidence. *Quaternary International*. 301:46–59.

Capriles JM, Albarracin-Jordan J, Lombardo U, Osorio D, Maley B, Goldstein ST, Herrera KA, Glascock MD, Domic AI, Veit H. 2016. High-altitude adaptation and late Pleistocene foraging in the Bolivian Andes. *Journal of Archaeological Science: Reports*. 6:463–474.

Cardich A. 1958. Los yacimientos de Lauricocha: nuevas interpretaciones de la prehistoria peruana (*Studia Praehistorica*, 1). Bueno Aires, Argentina: Centro Argentino de Estudios Prehistóricos.

Cardich A. 1964. Lauricocha: fundamentos para una prehistoria de los Andes Centrales. Centro Argentino de Estudios Prehistóricos.

Cartajena I. 2013. Faunal assemblages from the Middle Holocene: Environmental and cultural variability in the western slope of the Puna de Atacama. *Quaternary international*. 307:31–37.

Cartajena I, Núñez L, Grosjean M. 2007. Camelid domestication on the western slope of the Puna de Atacama, northern Chile. *anthropozoologica*. 42(2):155–173.

Chala-Aldana D, Bocherens H, Miller C, Moore K, Hodgins G, Rademaker K. 2017 Oct 27. Investigating mobility and highland occupation strategies during the Early Holocene at the Cuncaicha rock shelter through strontium and oxygen isotopes. *Journal of Archaeological Science: Reports*. doi:10.1016/j.jasrep.2017.10.023. [accessed 2018 Feb 14].
<http://www.sciencedirect.com/science/article/pii/S2352409X17301840>.

Conlee CA, Ogburn D. 2004. The Foundations of Power in the Prehispanic Andes: An Introduction. Archeological Papers of the American Anthropological Association. 14(1):1–12.

Crombé P, Aluwé K, Boudin M, Snoeck C, Messiaen L, Teetaert D. 2020. New evidence on the earliest domesticated animals and possible small-scale husbandry in Atlantic NW Europe. Sci Rep. 10(1):20083. doi:10.1038/s41598-020-77002-4.

DeNiro MJ. 1985. Postmortem preservation and alteration of in vivo bone collagen isotope ratios in relation to palaeodietary reconstruction. nature. 317(6040):806–809.

Díaz-Maroto P, Rey-Iglesia A, Cartajena I, Núñez L, Westbury MV, Varas V, Moraga M, Campos PF, Orozco-terWengel P, Marin JC. 2021. Ancient DNA reveals the lost domestication history of South American camelids in Northern Chile and across the Andes. Elife. 10:e63390.

Dillehay TD. 2014. Entangled knowledge: old trends and new thoughts in first South American studies. Paleoamerican odyssey.:377–396.

Dinerstein E, Olson D, Joshi A, Vynne C, Burgess ND, Wikramanayake E, Hahn N, Palminteri S, Hedao P, Noss R, et al. 2017. An Ecoregion-Based Approach to Protecting Half the Terrestrial Realm. BioScience. 67(6):534–545. doi:10.1093/biosci/bix014.

Dollfus O. 1978. Les Andes intertropicales: une mosaïque changeante. In: Annales. Histoire, Sciences Sociales. Vol. 33. Cambridge University Press. p. 895–903.

Fehren-Schmitz L, Llamas B, Lindauer S, Tomasto-Cagigao E, Kuzminsky S, Rohland N, Santos FR, Kaulicke P, Valverde G, Richards SM, et al. 2015. A Re-Appraisal of the Early Andean Human Remains from Lauricocha in Peru. PLOS ONE. 10(6):e0127141. doi:10.1371/journal.pone.0127141.

Galván VK, Martínez J, Cherkinsky A, Mondini M, Panarello H. 2016. Stable isotope analysis on human remains from the final Early Holocene in the southern Puna of Argentina: the case of Peñas de las Trampas 1.1. *Environmental Archaeology*. 21(1):1–10.

Haas J, Creamer W, Ruiz A. 2004. Power and the emergence of complex polities in the Peruvian Preceramic. *Archeological Papers of the American Anthropological Association*. 14(1):37–52.

Haas R, Watson J, Buonasera T, Southon J, Chen JC, Noe S, Smith K, Viviano Llave C, Eerkens J, Parker G. 2020. Female hunters of the early Americas. *Science Advances*. 6(45):eabd0310.

Higham T, Jacobi R, Basell L, Ramsey CB, Chiotti L, Nespoli R. 2011. Precision dating of the Palaeolithic: A new radiocarbon chronology for the Abri Pataud (France), a key Aurignacian sequence. *Journal of human evolution*. 61(5):549–563.

Hogg AG, Heaton TJ, Hua Q, Palmer JG, Turney CS, Southon J, Bayliss A, Blackwell PG, Boswijk G, Ramsey CB, et al. 2020. SHCal20 Southern Hemisphere Calibration, 0–55,000 Years cal BP. *Radiocarbon*. 62(4):759–778. doi:10.1017/RDC.2020.59.

Jodry MA, Santoro CM. 2017. Walking closer to the sky: High-altitude landscapes and the peopling of the New World. *Quaternary International*. 461:102–107.

Julien M, Lavallee D, Dietz M. 1981. Les sépultures préhistoriques de Telarmachay. Junin, Pérou. *Bulletin de l’Institut Français d’Études Andines*. 10(1):85–99.

Julien M, Vaughan P, Lavallée D. 1987. Armes et outils emmanchés à Telarmachay. Présomptions et indices. *Publications de la Maison de l’Orient et de la Méditerranée*. 15(1):287–295.

Kanezaki Y, Omori T, Tsurumi E. 2021. Emergence and Development of Pottery in the Andean Early Formative Period: New Insights from an Improved Wairajirca Pottery Chronology at the Jancau Site in the Huánuco Region, Peru. *Latin American Antiquity*. 32(2):239–254.

Karakostis FA, Reyes-Centeno H, Franken M, Hotz G, Rademaker K, Harvati K. 2021. Biocultural evidence of precise manual activities in an Early Holocene individual of the high-altitude Peruvian Andes. *American Journal of Physical Anthropology*. 174(1):35–48.

Kaulicke P. 1980. Der Abri Uchkumachay und seine zeitliche Stellung innerhalb der lithischen Perioden Perus. *Beiträge zur Allgemeinen und Vergleichenden Archäologie*. 2:429–458.

Kaulicke P. 1999. Contribuciones hacia la cronología del Periodo Arcaico en las punas de Junín. *Boletín de Arqueología PUCP*. (3):307–324.

Keatinge RW. 1988. Peruvian prehistory: An overview of pre-Inca and Inca society.

Kent JD. 1982. The domestication and exploitation of the South American camelids: methods of analysis and their application to circum-lacustrine archaeological sites in Bolivia and Peru. Washington University.

Lavallée D. 1988. L'occupation préhistorique de l'abri de Telarmachay (Pérou) - un aspect de la néolithisation andine. *crai*. 132(2):266–288. doi:10.3406/crai.1988.14604.

Lavallée D. 1990. Analyse palethnologique d'un habitat préhistorique andin: l'abri de Telarmachay, (Junín, Pérou). *Revista de Arqueología Americana*. (2):55–88.

Lavallée D. 1995. Promesse d'Amérique: La préhistoire de l'Amérique du Sud. Hachette.

Lavallée D, Julien M. 1980. Un aspect de la préhistoire andine : l'exploitation des camélidés et des cervidés au formatif dans l'abri de Telarmachay, Junin, Pérou. *jsa*. 67(1):97–124. doi:10.3406/jsa.1980.2189.

Lavallée D, Julien M, Wheeler J. 1985. Telarmachay: chasseurs et pasteurs préhistoriques des Andes. Paris, France: Ed. Recherche sur les Civilisations.

Lindauer S, Tomasto-Cagigao E, Fehren-Schmitz L. 2015. The skeletons of Lauricocha: new data on old bones. *Journal of Archaeological Science: Reports*. 4:387–394.

Loyola R, Núñez L, Aschero C, Cartajena I. 2017. Tecnología lítica del pleistoceno final y la colonización del salar de punta negra (24, 5° S), desierto de atacama. *Estudios atacameños*.(55):5–34.

Lynch TF, Gillespie R, Gowlett JA, Hedges RE. 1985. Chronology of Guitarrero cave, Peru. *Science*. 229(4716):864–867.

Marsh EJ. 2015. The emergence of agropastoralism: Accelerated ecocultural change on the Andean altiplano, 3540–3120 cal BP. *Environmental Archaeology*. 20(1):13–29.

Marsh EJ, Bruno MC, Fritz SC, Baker P, Capriles JM, Hastorf CA. 2018. IntCal, SHCal, or a mixed curve? Choosing a ¹⁴C calibration curve for archaeological and paleoenvironmental records from tropical South America. *Radiocarbon*. 60(3):925–940.

Marsh EJ, Kidd R, Ogburn D, Durán V. 2017. Dating the expansion of the Inca empire: Bayesian models from Ecuador and Argentina. *Radiocarbon*. 59(1):117–140.

Meinekat SA, Miller CE, Rademaker K. 2021. A site formation model for Cuncaicha rock shelter: Depositional and postdepositional processes at the high-altitude keysite in the Peruvian Andes. *Geoarchaeology*.

Mengoni Goñalons GL. 2008. Camelids in ancient Andean societies: A review of the zooarchaeological evidence. *Quaternary International*. 185(1):59–68.
doi:10.1016/j.quaint.2007.05.022.

Mengoni Goñalons GL, Yacobaccio HD. 2006. The domestication of South American camelids. In: Documenting Domestication—New Genetic and Archaeological Paradigms. University of California Press Berkeley-Los Angeles-London. p. 228–244.

Metcalf JL, C Turney, T Barnett, F Martin, SC Bray, JT Vilstrup, L Orlando, R Salas-Gismondi, D Loponte, M Medina, M de Nigris, T Civalero, PM Fernandez, A Gasco, V Duran, KL Seymour, C Otaola, A Gil, R Paunero, FJ. Prevosti, CJA Bradshaw, JC Wheeler, L Borrero, JJ Austin and A Cooper. 2016. Synergistic roles of climate warming and human occupation in Patagonian megafaunal extinctions during the Last Deglaciation. *Science advances*. 2(6):e1501682.

Moore K, Rademaker K. 2016. Hunters paradise or hypoxic wasteland. The human ecology of early high-elevation sites in the Peruvian Andes The Role of High Altitude Landscapes in the Peopling of the New World Society for American Archaeology, Orlando, Florida.

Moore KM. 1989. Hunting and the origins of herding in Peru [PhD Thesis]. University of Michigan.

Moore KM. 1998. Measures of mobility and occupational intensity in highland Peru. Seasonality and Sedentism, Archaeological Perspectives from Old and New World Sites.:181–197.

Nakatsuka N, Lazaridis I, Barbieri C, Skoglund P, Rohland N, Mallick S, Posth C, Harkins-Kinkaid K, Ferry M, Harney É. 2020. A paleogenomic reconstruction of the deep population history of the Andes. *Cell*. 181(5):1131–1145.

Oberlin C, Valladas H. 2015. Datation par le Radiocarbone de la fraction organique de l'os. M BALASSE, Y DAUPHIN, JP BRUGAL, E-M GEIGL, C OBERLIN et I REICHE (éd), Messages d'Os Archéométrie du squelette animal et humain, Éditions des archives contemporaines, Paris.:295–314.

Ogburn DE. 2012. Reconceiving the chronology of Inca imperial expansion. *Radiocarbon*. 54(2):219–237.

Olson DM, Dinerstein E, Wikramanayake ED, Burgess ND, Powell GVN, Underwood EC, D'amico JA, Itoua I, Strand HE, Morrison JC, et al. 2001. Terrestrial Ecoregions of the World: A New Map of Life on Earth: A new global map of terrestrial ecoregions provides an innovative tool for conserving biodiversity. *BioScience*. 51(11):933–938. doi:10.1641/0006-3568(2001)051[0933:TEOTWA]2.0.CO;2.

Ortiz V, Lynch T, The 81st Annual Meeting of the Society for American Archaeology. 2016. Quishqui Punku (PA 3-170), Early Use of High Altitude Sites in the Callejon de Huaylas (Ancash), Peru.

Osorio D, Capriles JM, Ugalde PC, Herrera KA, Sepúlveda M, Gayo EM, Latorre C, Jackson D, De Pol-Holz R, Santoro CM. 2017. Hunter-Gatherer Mobility Strategies in the High Andes of Northern Chile during the Late Pleistocene-Early Holocene Transition (ca. 11,500–9500 CAL B.P.). *Journal of Field Archaeology*. 42(3):228–240. doi:10.1080/00934690.2017.1322874.

Osorio D, Steele J, Sepúlveda M, Gayo EM, Capriles JM, Herrera K, Ugalde P, De Pol-Holz R, Latorre C, Santoro CM. 2017. The Dry Puna as an ecological megapatch and the peopling of South America: Technology, mobility, and the development of a late Pleistocene/early Holocene Andean hunter-gatherer tradition in northern Chile. *Quaternary International*. 461:41–53.

Pereyra Parra A, López Carranza E, Lavallée D. 1982. Datación por termoluminiscencia de tiestos cerámicos antiguos provenientes de Telarmachay. *Bulletin de l’Institut Français d’Études Andines*. 11(1):91–95.

Pereyra Parra A, López Carranza E, Lavallée D. 1983. Datacion por termoluminiscencia de tiestos ceramicos formativos provenientes de Telarmachay: fechas revisadas. *Bulletin de l’Institut Français d’Études Andines*. 12(3):115–118.

Pozorski S, Pozorski T. 2008. Early cultural complexity on the coast of Peru. In: *The handbook of south American archaeology*. Springer. p. 607–631.

Pulgar Vidal J. 1981. *Geografía del Perú: las ocho regiones naturales del Perú*. Editorial Universo, Lima.

Rademaker K, Bromley GR, Sandweiss DH. 2013. Peru archaeological radiocarbon database, 13,000–7000 14C BP. *Quaternary International*. 301:34–45.

Rademaker K, Hodgins G. 2018. Exploring the chronology of occupations and burials at Cuncaicha rockshelter, Peru. *New Perspectives on the Peopling of the Americas*, Kerns Verlag, Tuebingen.:107–124.

Rademaker K, Hodgins G, Moore K, Zarrillo S, Miller C, Bromley GR, Leach P, Reid D, Álvarez WY, Sandweiss DH. 2016. Cuncaicha Rockshelter, a Key Site for Understanding Colonization of the High Andes: Reply to Capriles et al. *Current Anthropology*. 57(1):101–103.

Rademaker K, Hodgins G, Moore K, Zarrillo S, Miller C, Bromley GR, Leach P, Reid DA, Álvarez WY, Sandweiss DH. 2014. Paleoindian settlement of the high-altitude Peruvian Andes. *Science*. 346(6208):466–469.

Rademaker K, Moore K. 2019. Variation in the Occupation Intensity of Early Forager Sites of the Andean Puna. p. 76–118.

Rademaker K, Moore K, Lemke A. 2018. Variation in the Occupation Intensity of Early Forager Sites of the Andean Puna. Implications for Settlement and Adaptation. Foraging in the past: Archaeological studies of hunter-gatherer diversity.:76–118.

Ramsey CB, Lee S. 2013. Recent and planned developments of the program OxCal. Radiocarbon. 55(2):720–730.

Reimer PJ, Austin WE, Bard E, Bayliss A, Blackwell PG, Ramsey CB, Butzin M, Cheng H, Edwards RL, Friedrich M. 2020. The IntCal20 Northern Hemisphere radiocarbon age calibration curve (0–55 cal kBP). Radiocarbon. 62(4):725–757.

Rick JW. 1980. Prehistoric hunters of the high Andes. New York: Academic Press (Studies in archaeology).

Rick JW, Moore KM. 1999. El Precerámico de las punas de Junín: el punto de vista desde Panaulauca. Boletín de Arqueología PUCP.(3):263–296.

Salcedo Camacho L E, Marcos S. 2019. Central Andes: Prehispanic Hunter-Gatherers.

Santoro CM, Standen VG, Arriaza BT, Dillehay TD. 2005. Archaic funerary pattern or postdepositional alteration? The Patapatane Burial in the Highlands of South Central Andes. Latin American Antiquity. 16(3):329–346.

Seltzer GO, Rodbell DT, Baker PA, Fritz SC, Tapia PM, Rowe HD, Dunbar RB. 2002. Early warming of tropical South America at the last glacial-interglacial transition. Science. 296(5573):1685–1686.

Shockley BJ. 2009. New Pleistocene cave faunas of the Andes of central Peru: radiocarbon ages and the survival of low latitude, Pleistocene DNA. *Palaeontologia Electronica*. 12(3):1–15.

Stansell ND, Rodbell DT, Abbott MB, Mark BG. 2013. Proglacial lake sediment records of Holocene climate change in the western Cordillera of Peru. *Quaternary Science Reviews*. 70:1–14.

Tosi JA. 1960. Zonas de vida natural en el Perú: memoria explicativa sobre el mapa ecológico del Perú. IICA Biblioteca Venezuela.

Troll C. 1968. The cordilleras of the tropical Americas, aspects of climatic, phytogeographical and agrarian ecology. In: *Colloquium Geographicum* (Univ. Bonn). Vol. 9. p. 15–56.

Van Klinken GJ. 1999. Bone collagen quality indicators for palaeodietary and radiocarbon measurements. *Journal of archaeological science*. 26(6):687–695.

Vaughn KJ. 2006. Craft production, exchange, and political power in the pre-Incaic Andes. *Journal of Archaeological Research*. 14(4):313–344.

Wheeler JC. 1985. De la chasse à l'élevage. Telarmachay Chasseurs et pasteurs préhistoriques des Andes I CNRS, Paris, pp61–79.

Wheeler JC. 1999. Patrones prehistóricos de utilización de los camélidos sudamericanos. *Boletín de arqueología pucp.*(3):297–305.

Wheeler Pires-Ferreira J, Pires-Ferreira E, Kaulicke P. 1976. Preceramic animal utilization in the Central Peruvian Andes. *Science*. 194(4264):483–490.

Wing ES. 1972. Utilization of Animal Resources in the Peruvian Andes. In: Seiichi I, Terada K, editors. *Andes 4: Excavations at Kotosh, Peru, 1963 and 1966*. Tokyo: University of Tokyo Press. p. 327–352.

Wing ES. 1975. Informe preliminar acerca de los restos de fauna de la cueva de Pachamachay en Junín, Perú. *Revista del Museo Nacional*. 41:79–80.

Woods A, Rodbell DT, Abbott MB, Hatfield RG, Chen CY, Lehmann SB, McGee D, Weidhaas NC, Tapia PM, Valero-Garcés BL. 2020. Andean drought and glacial retreat tied to Greenland warming during the last glacial period. *Nature communications*. 11(1):1–7.

Yacobaccio HD. 2017. Peopling of the high Andes of northwestern Argentina. *Quaternary International*. 461:34–40.

Zazzo A, Lepetz S, Magail J, Gantulga J-O. 2019. High-precision dating of ceremonial activity around a large ritual complex in Late Bronze Age Mongolia. *antiquity*. 93(367):80–98.

Appendix(es):

Appendix 1: Telarmachay chronostratigraphy based on charcoal (Lavallée and Julien 1980; Lavallée et al. 1985) and SAC bones (Metcalf et al. 2016) after their calibration with the “Shcal20” curve (Hogg et al. 2020) in BP. Moreover, according to one of us (JCW), SAC bones samples highlighted in bold here (Metcalf et al. (2016)'s samples) have been erroneously identified as coming from Layer IV in Metcalf et al. (2016).

			¹⁴ C age (BP)		Calibrated range (2 sigmas)		
Layer dating boundaries	Square meter unit	Samples lab code	Raw age	Error	Start (BP)	End (BP)	%
Layer II, around 2800-2000 BP	?	R_Date II Gif-3772	2190	100	2350	1892	95.4
	?	R_Date IIsup Gif-3774	2120	100	2330	1832	95.4
	?	R_Date IImoy Gif-3773	2280	100	2689	1938	95.4
	?	R_Date IIinf Gif-4187	2600	90	2847	2359	95.4
Layer III, around 3800-2800 BP	?	R_Date IIIsup Gif-4188	3410	100	3873	3389	95.4
	?	R_Date IIIinf Gif-4189	3470	100	3970	3450	95.4
Layer IV, around 5000/4500 - 3800 BP	B7	R_Date IVa Gif-4835	3680	100	4288	3650	95.4
	C8	R_Date IVa Gif-4836	3700	100	4343	3698	95.4
	C11	R_Date IVa Gif-4834	3910	110	4785	3929	95.4
	E9	R_Date IVc Gif-5045	4420	110	5320	4647	95.4
	C6	R_Date IVa Gif-4837	4470	110	5445	4826	95.4
Layer V sup., around 5700-5000 BP	B6	R_Date Va Gif-5393	4430	70	5284	4845	95.4
Layer V inf., around 6800-5700 BP	B6	R_Date Va-b Lv-1190/1	4910	80	5889	5329	95.4
	A6-7	R_Date Vc Lv-1276	5000	80	5908	5494	95.4
	C6	R_Date Va Gif-5047	5190	110	6195	5607	95.4
	A7	R_Date Vb-c Gif-5391	5320	120	6304	5750	95.4
	E10	R_Date Va Gif-5046	5370	110	6391	5898	95.4
	D9	R_Date Vb Lv-1134	5700	65	6627	6305	95.4
	E9	R_Date Vc Lv-1192	6110	80	7165	6735	95.4
	E8	R_Date Vc Gif-5392	6780	130	7922	7366	95.4
Layer VI, around 7200-6800 BP	?	R_Date TVI OXA-20857	6690	40	7591	7430	95.4
	?	R_Date TVI OXA-20856	6220	40	7245	6949	95.4
	?	R_Date TVI OXA-20855	6970	40	7919	7673	95.4
	?	R_Date TVI OXA-20854	6965	40	7919	7671	95.4
	B8	R_Date VIa Gif-5390	4220	110	5036	4415	95.4
	C11	R_Date VIa Gif-5394	5320	110	6299	5755	95.4
	D7	R_Date VIa Gif-5388	5580	120	6632	6005	95.4
	D10	R_Date VIa Lv-1277	7150	90	8169	7731	95.4
	C9	R_Date VIIa Lv-1278	7140	60	8028	7785	95.4

Layer VII, around 9000-7200 BP	C11	R_Date VIIa Gif-5389	7250	140	8344	7752	95.4
	C8	R_Date VIIa Lv-1193	7620	60	8539	8206	95.4
	C11	R_Date VIIb Lv-1279	8810	65	10130	9549	95.4
	C6	R_Date VIIb Pucp-1825	12040	120	14161	13529	95.4

Appendix 2: Radiocarbon age obtained on camelid bone collagen from Telarmachay (Cal BP 2 sigmas) and calibrated dates (Cal BP) with the (SHcal20) curve (Hogg et al. 2020); elemental carbon (C%) and nitrogen (N%) contents, atomic C/N, and extraction yields of bone collagen.

Layer	Square meter unit	anatomical part	taxa	ECHo	complete lab code	age (yr BP)	error	From (yr BP)	To (yr BP)	median	Yield (%)	%C	%N	C:N ratio
II	C6	talus	camelid	4226.1.1	tel-II-cam-4226.1.1	3 420	25	3812	3494	3619	22.9	43.8	15.9	3.21
II	E8	phalange	camelid	4224.1.1	tel-II-cam-4224.1.1	3 900	25	4411	4155	4290	17	43.0	15.7	3.20
II	D6	calcaneus	camelid	4225.1.1	tel-II-cam-4225.1.1	4 065	25	4613	4415	4486	16.3	43.8	15.9	3.21
III	B7?	talus	camelid	4221.1.1	tel-III-cam-4221.1.1	3 545	25	3882	3692	3776	24.6	44.1	16.0	3.22
III	C6	talus	camelid	4222.1.1	tel-III-cam-4222.1.1	3 920	25	4417	4158	4320	20.4	43.5	15.7	3.22
III	F10	talus	camelid	4223.1.1	tel-III-cam-4223.1.1	4 055	25	4575	4414	4481	20	43.6	15.9	3.21
III	D6	talus	camelid	4220.1.1	tel-III-cam-4220.1.1	5 140	30	5929	5744	5817	12	42.9	15.7	3.19
IV	B11?	talus	camelid	4213.1.1	tel-IV-cam-4213.1.1	4 240	121	4849	4589	4734	22.3	44.3	16.1	3.21
IV	A6	talus	camelid	4215.1.1	tel-IV-cam-4215.1.1	4 750	30	5579	5322	5439	8.1	42.4	15.4	3.21
IV	D6	mandible	camelid	4219.1.1	tel-IV-cam-4219.1.1	5 040	25	5894	5604	5731	17.7	41.6	15.1	3.22
IV	D11	mandible	camelid	4217.1.1	tel-IV-cam-4217.1.1	5 120	30	5918	5735	5815	14.8	42.8	15.4	3.23

IV	D11	mandible	camelid	4216.1.1	tel-IV-cam-4216.1.1	5 210	30	6106	5759	5934	14.7	42.8	15.6	3.21
IV	D6	mandible	camelid	4218.1.1	tel-IV-cam-4218.1.1	5 215	30	6109	5761	5939	7.5	41.2	15.0	3.22
IV	E6	talus	camelid	4214.1.1	tel-IV-cam-4214.1.1	5 395	30	6279	6001	6140	19.7	43.5	15.7	3.23
IV	E11	talus	camelid	4212.1.1	tel-IV-cam-4212.1.1	5 855	30	6734	6499	6626	20.2	41.9	15.3	3.20
V	A7	talus	camelid	4208.1.1	tel-V-cam-4208.1.1	4 160	25	4820	4526	4665	24.8	43.9	16.0	3.21
V	E7	talus	camelid	4206.1.1	tel-V-cam-4206.1.1	5 435	25	6290	6014	6220	19.8	43.2	15.6	3.23
V	D10	talus	camelid	4205.1.1	tel-V-cam-4205.1.1	5 780	30	6650	6443	6542	20.8	43.6	15.8	3.22
V	E6	talus	camelid	4207.1.1	tel-V-cam-4207.1.1	5 875	25	6744	6505	6654	16.2	43.2	15.6	3.23
V	E6	talus	camelid	4209.1.1	tel-V-cam-4209.1.1	5 935	25	6827	6642	6716	15.6	43.1	15.6	3.22
V	E7	mandible	camelid	4211.1.1	tel-V-cam-4211.1.1	6 095	30	7150	6792	6910	14.7	43.3	15.6	3.24
VI	B7	talus	camelid	4199.1.1	tel-VI-cam-4199.1.1	6 185	30	7163	6938	7050	11.8	42.9	15.5	3.23
VI	B7	talus	camelid	4203.1.1	tel-VI-cam-4203.1.1	6 280	30	7260	7011	7167	14.9	43.4	15.8	3.21
VI	A6	talus	camelid	4202.1.1	tel-VI-cam-4202.1.1	6 290	30	7263	7016	7191	17.1	42.1	15.3	3.20
VI	locus_e 7	NA	camelid	4204.1.1	tel-VI-cam-4204.1.1	6 920	30	7830	7619	7715	13.3	43.3	15.7	3.22
VI		C7	camelid	4201.1.1	tel-VI-cam-4201.1.1	6 935	30	7836	7663	7727	22	43.5	15.8	3.21
VI	C7	talus	camelid	4200.1.1	tel-VI-cam-4200.1.1	7 010	30	7927	7695	7804	11.8	42.5	15.5	3.20
VII	B6	talus	camelid	4193.1.1	tel-VII-cam-4193.1.1	6 870	30	7744	7584	7662	18.7	41.6	14.9	3.25
VII	B7	talus	camelid	4196.1.1	tel-VII-cam-4196.1.1	6 975	30	7916	7678	7763	22.2	43.3	15.7	3.21
VII	B11	talus	camelid	4194.1.1	tel-VII-cam-4194.1.1	7 110	30	7974	7794	7894	25.3	41.9	15.1	3.25
VII	B6	talus	camelid	4195.1.1	tel-VII-cam-4195.1.1	7 320	30	8177	8017	8102	22.6	43.2	15.7	3.21

VII	E8	phalange	camelid	4197.1.1	tel-VII-cam-4197.1.1	7 395	30	8316	8029	8143	20.7	43.4	15.8	3.21
VII	A6	talus	camelid	4198.1.1	tel-VII-cam-4198.1.1	7 860	30	8724	8460	8598	23.1	44.0	16.0	3.22

Appendix 3: outlier probability results from the Bayesian age model using a t-type outlier model method with prior probabilities set at 0.05. In the first column are the prior outlier settings, and in the next column are the posterior probabilities obtained after the modelling of the results. Samples that have a greater than 5% and 20 % probability of being misplaced in the proposed stratigraphy are highlighted in black.

ECHo	Prior	Posterior	Model	Type
4193.1.1	5	84	General	t
4194.1.1	5	3	General	t
4195.1.1	5	2	General	t
4197.1.1	5	2	General	t
4198.1.1	5	48	General	t
4196.1.1	5	20	General	t
4202.1.1	5	3	General	t
4203.1.1	5	2	General	t
4199.1.1	5	4	General	t
4200.1.1	5	7	General	t
4201.1.1	5	2	General	t
4204.1.1	5	3	General	t
OXA-20854	5	4	General	t

OXA-20855	5	3	General	t
OXA-20856	5	3	General	t
OXA-20857	5	3	General	t
4208.1.1	5	100	General	t
4209.1.1	5	2	General	t
4205.1.1	5	3	General	t
4206.1.1	5	35	General	t
4207.1.1	5	2	General	t
4211.1.1	5	11	General	t
4212.1.1	5	93	General	t
4213.1.1	5	67	General	t
4214.1.1	5	7	General	t
4215.1.1	5	11	General	t
4216.1.1	5	2	General	t
4217.1.1	5	2	General	t
4218.1	5	2	General	t
4219.1.1	5	4	General	t
4220.1.1	5	100	General	t
4221.1.1	5	2	General	t
4222.1.1	5	2	General	t
4223.1.1	5	2	General	t
4224.1.1	5	3	General	t
4225.1.1	5	6	General	t

4226.1.1	5	6	General	t
----------	---	---	---------	---

Appendix 4: Radiocarbon age obtained on camelid bone collagen from Telarmachay (Cal BP 2 sigmas) and calibrated dates (Cal BP) with the mixed curve IntCal20 (Reimer et al. 2020) and SHcal20 (Hogg et al. 2020) approach (Buck 2004; Ogburn 2012; Marsh et al. 2017; Marsh et al. 2018) compared to radiocarbon age obtained with the SHcal20 curve (Hogg et al. 2020):

a. **calibrated dates:**

Layer	ECHo	age (yr BP)	error	From (yr BP) mixed curve	To (yr BP) mixed curve	%	From (yr BP) SHcal20 curve	To (yr BP) SHcal20 curve
II	4226.1.1	3 420	25	3812	3499	95.4	3812	3494
II	4224.1.1	3 900	25	4413	4159	95.4	4411	4155
II	4225.1.1	4 065	25	4777	4417	95.4	4613	4415
III	4221.1.1	3 545	25	3881	3699	95.4	3882	3692
III	4222.1.1	3 920	25	4419	4186	95.4	4417	4158
III	4223.1.1	4 055	25	4575	4417	95.4	4575	4414
III	4220.1.1	5 140	30	5934	5746	95.4	5929	5744
IV	4213.1.1	4 240	121	4852	4624	95.4	4849	4589
IV	4215.1.1	4 750	30	5580	5324	95.4	5579	5322
IV	4219.1.1	5 040	25	5895	5608	95.4	5894	5604
IV	4217.1.1	5 120	30	5919	5745	95.4	5918	5735
IV	4216.1.1	5 210	30	6108	5772	95.4	6106	5759

IV	4218.1.1	5 215	30	6110	5895	95.4	6109	5761
IV	4214.1.1	5 395	30	6280	6005	95.4	6279	6001
IV	4212.1.1	5 855	30	6739	6503	95.4	6734	6499
V	4208.1.1	4 160	25	4822	4531	95.4	4820	4526
V	4206.1.1	5 435	25	6293	6032	95.4	6290	6014
V	4205.1.1	5 780	30	6654	6451	95.4	6650	6443
V	4207.1.1	5 875	25	6744	6561	95.4	6744	6505
V	4209.1.1	5 935	25	6795	6659	95.4	6827	6642
V	4211.1.1	6 095	30	7151	6796	95.4	7150	6792
VI	4199.1.1	6 185	30	7161	6955	95.4	7163	6938
VI	4203.1.1	6 280	30	7261	7021	95.4	7260	7011
VI	4202.1.1	6 290	30	7266	7022	95.4	7263	7016
VI	4204.1.1	6 920	30	7831	7662	95.4	7830	7619
VI	4201.1.1	6 935	30	7833	7671	95.4	7836	7663
VI	4200.1.1	7 010	30	7928	7709	95.4	7927	7695
VII	4193.1.1	6 870	30	7750	7590	95.4	7744	7584
VII	4196.1.1	6 975	30	7916	7684	95.4	7916	7678
VII	4194.1.1	7 110	30	7976	7800	95.4	7974	7794
VII	4195.1.1	7 320	30	8175	8024	95.4	8177	8017
VII	4197.1.1	7 395	30	8319	8034	95.4	8316	8029

VII	4198.1.1	7 860	30	8755	8536	95.4	8724	8460
-----	----------	-------	----	------	------	------	------	------

b. *Bayesian modelings:*

SHcal20 curve:

Name	Unmodelled d (BP)			Modelled (BP)			Indices				
	From	to	%	from	to	%	Acomb	A	L	P	C
Amodel 11.3											
Aoverall 12"											
Boundary TII-II End				4387	3027	95.44					27.5
Interval Duration TII-II				113	1991	95.44					36.5
Span Span of TII-II				70	1385	95.44					41.2
R_Date TII47- MUSE21074	3813	3494	95.44	4498	3491	95.44		87.2		87.3	51.3
R_Date TII7- MUSE21073	4778	4415	95.44	4611	4413	95.44		108.2		96.9	95.7
R_Date TII23- MUSE21070	4411	4155	95.44	4414	4152	95.44		101.3		96.1	87.3
R_Date TIII50- MUSE21077	4576	4414	95.44	4575	4412	95.44		106.7		97.4	96.5
R_Date TIII57- MUSE21076	4416	4158	95.44	4417	4157	95.44		103.3		98	92.3
R_Date TIII56- MUSE21075	3882	3692	95.44	4471	3644	95.44		96.3		91.6	59.6
R_Date TIII59- MUSE21069	5929	5745	95.44	4974	3470	95.44		6.2		0.7	71.5
Phase TIII-II			95.44			95.44					
Boundary TIII-II Start			95.44	5193	4431	95.44					84.2
Interval between TIV and TIII-II			95.44	0	1036	95.44					39.9

Boundary TIV End			95.44	5871	4515	95.44					11.8
Interval Duration TIV			95.44	214	1907	95.44					18.1
Span Span of TIV			95.44	132	1824	95.44					18
R_Date TIVCDF_109_2- MUSE21092	5894	5604	95.44	5896	5604	95.44		100.9		96.9	96.2
R_Date TIVCDF_109_1- MUSE21091	6108	5761	95.44	6107	5759	95.44		104.5		97.9	98.1
R_Date TIVCDF_105_2- MUSE21090	5917	5735	95.44	5924	5726	95.44		102.2		97.3	97.9
R_Date TIVCDF_105_1- MUSE21089	6106	5759	95.44	6106	5756	95.44		103.9		97.4	98
R_Date TIV40- MUSE21080	5579	5322	95.44	6026	5317	95.44		87		86.3	74.7
R_Date TIV38- MUSE21079	6278	6001	95.44	6279	5918	95.44		90.6		93.2	95.2
R_Date TIV37- MUSE21078	4848	4587	95.44	6133	4622	95.44		50		41.4	3.8
R_Date TIV42- MUSE21068	6734	6499	95.44	6590	5267	95.44		8.2		5.3	65.4
Phase TIV			95.44			95.44					
Boundary TIV Start			95.44	6602	5956	95.44					91.4
Interval between TV and TIV			95.44	0	421	95.44					94.6
Boundary TV End			95.44	6646	6050	95.44					84.7
Interval Duration TV			95.44	190	919	95.44					86.5
Span Span of TV			95.44	140	762	95.44					82.8
R_Date TVCDF_110- MUSE21093	7150	6792	95.44	6994	6550	95.44		80.7		87.8	98.2

R_Date TV17-MUSE21083	6744	6506	95.44	6745	6504	95.44		104.6	97.9	98.9
R_Date TV12-MUSE21082	6290	6012	95.44	6884	6122	95.44		75.4	61	91
R_Date TV9-MUSE21081	6651	6413	95.44	6665	6411	95.44		99.1	96.7	96.2
R_Date TV24-MUSE21066	6827	6642	95.44	6832	6635	95.44		103.1	97.4	99.1
R_Date TV34-MUSE21065	4820	4526	95.44	6913	6163	95.44		5.6		84.8
Phase TV			95.44			95.44				
Boundary TV Start			95.44	7058	6720	95.44				98.8
Interval between TVI and TV			95.44	0	276	95.44				99.4
Boundary TVI End			95.44	7141	6880	95.44				98.5
Interval Duration TVI			95.44	631	952	95.44				98.9
Span Span of TVI			95.44	589	833	95.44				98.3
R_Date TVI OXA-20857	7603	7430	95.44	7613	7428	95.44		101.4	96.3	98.6
R_Date TVI OXA-20856	7245	6949	95.44	7252	6984	95.44		103.1	97	98.3
R_Date TVI OXA-20855	7918	7674	95.44	7836	7666	95.44		111.1	97	98.1
R_Date TVI OXA-20854	7918	7671	95.44	7836	7664	95.44		111.8	97	98.4
R_Date TVICDF_113-MUSE21094	7829	7619	95.44	7791	7618	95.44		108.8	98.1	98.6
R_Date TVI88-MUSE21086	7835	7663	95.44	7837	7057	95.44		105.2	93.5	87.9
R_Date TVI86-MUSE21085	7926	7695	95.44	7870	7203	95.44		86.8	92.8	94.1

R_Date TVI83-MUSE21084	7163	6937	95.44	7238	6951	95.44		105.2	96	98.3
R_Date TVI82-MUSE21064	7258	7012	95.44	7262	7016	95.44		107.1	97.2	98.3
R_Date TVI81-MUSE21063	7262	7016	95.44	7266	7019	95.44		107.4	97.5	98.3
Phase TVI			95.44			95.44				
Boundary TVI Start			95.44	7886	7719	95.44				98
Interval between TVII and TVI			95.44	0	116	95.44				99.1
Boundary TVII End			95.44	7939	7734	95.44				96.6
Interval Duration TVII			95.44	145	1240	95.44				84.6
Span Span of TVII			95.44	119	904	95.44				83.6
R_Date TVII72-MUSE21088	7916	7677	95.44	8218	7749	95.44		42.8	78.4	96
R_Date TVII1-MUSE21087	8723	8460	95.44	8718	7816	95.44		60.7	55.8	84.1
R_Date TVII42-MUSE21072	8317	8028	95.44	8316	8025	95.44		105.4	97.5	97.8
R_Date TVII71-MUSE21071	8177	8017	95.44	8179	8011	95.44		101.9	98	98.4
R_Date TVII74-MUSE21062	7973	7794	95.44	8012	7832	95.44		102.4	96.7	98.3
R_Date TVII69-MUSE21061	7744	7584	95.44	8659	7738	95.44		5.6	12.8	46.3
Phase TVII			95.44			95.44				
Boundary TVII Start			95.44	9025	8046	95.44				72.7
Sequence Telarmachay			95.44			95.44				
U(0,4)	3.98986e-17	4	95.44	2.3	3.1	95.44		100		22.4
T(5)	-2.65	2.65	95.44			95.44				77.1

Outlier_Model General				-1921	2196	95.44					37.7
Curve SHCal20											

Mixed curve:

Name	Unmodell ed (BP)			Modelled (BP)			Indices				
	From	to	%	from	to	%	Acomb	A	L	P	C
Amodel 7.6											
Aoverall 7.7"											
Boundary TII-II End				3807	3043	95.4					92.6
Interval Duration TII-II			95.4	751	2316	95.4					38
Span Span of TII-II			95.4	633	2198	95.4					40.9
R_Date TII47- MUSE21074	3813	3569	95.4	3824	3496	95.4		96.8		95.4	95.8
R_Date TII7- MUSE21073	4781	4420	95.4	4614	4415	95.4		100.7		96.5	97
R_Date TII23- MUSE21070	4414	4185	95.4	4414	4155	95.4		94		96.6	97.9
R_Date TIII50- MUSE21077	4577	4419	95.4	4574	4416	95.4		102.7		97.2	96.8
R_Date TIII57- MUSE21076	4416	4245	95.4	4419	4156	95.4		93.8		95.9	96.3
R_Date TIII56- MUSE21075	3891	3699	95.4	3895	3692	95.4		95.1		96.6	97.3
R_Date TIII59- MUSE21069	5982	5750	95.4	5820	3561	95.4		8		3.7	4.9
Phase TIII-II			95.4			95.4					
Boundary TIII-II Start			95.4	5849	4442	95.4					18.3
Interval between TIV and TIII-II			95.4	0	1048	95.4					43.6

Boundary TIV End			95.4	5885	4547	95.4					1.7
Interval Duration TIV			95.4	160	1898	95.4					3.9
Span Span of TIV			95.4	112	1834	95.4					4
R_Date TIVCDF_109_2- MUSE21092	5895	5658	95.4	5897	5607	95.4		96.1	96.7		55.2
R_Date TIVCDF_109_1- MUSE21091	6105	5904	95.4	6109	5761	95.4		98.7	96.5		98.2
R_Date TIVCDF_105_2- MUSE21090	5922	5748	95.4	5924	5739	95.4		95.2	97.2		71.5
R_Date TIVCDF_105_1- MUSE21089	6102	5903	95.4	6108	5759	95.4		97.7	96.3		98.4
R_Date TIV40- MUSE21080	5580	5326	95.4	6057	5321	95.4		84.3	80.4		14.6
R_Date TIV38- MUSE21079	6282	6008	95.4	6281	5871	95.4		59	91.5		73.5
R_Date TIV37- MUSE21078	4853	4647	95.4	6144	4649	95.4		31.6	26.3		1.7
R_Date TIV42- MUSE21068	6740	6556	95.4	6604	5368	95.4		7.4	8.6		48.8
Phase TIV			95.4			95.4					
Boundary TIV Start			95.4	6626	5968	95.4					56.4
Interval between TV and TIV			95.4	0	426	95.4					90.9
Boundary TV End			95.4	6655	6050	95.4					58.5
Interval Duration TV			95.4	166	931	95.4					60.9
Span Span of TV			95.4	125	773	95.4					56.5
R_Date TVCDF_110- MUSE21093	7152	6799	95.4	6996	6621	95.4		67	88.7		95.9

R_Date TV17-MUSE21083	6745	6565	95.4	6747	6555	95.4		90.5	97.2	98.8
R_Date TV12-MUSE21082	6289	6126	95.4	6879	6126	95.4		62.7	58.6	72.6
R_Date TV9-MUSE21081	6659	6458	95.4	6670	6411	95.4		94.6	95.7	89.7
R_Date TV24-MUSE21066	6826	6666	95.4	6828	6652	95.4		100	98.1	98.8
R_Date TV34-MUSE21065	4824	4535	95.4	6921	6177	95.4		5.4		79.5
Phase TV			95.4			95.4				
Boundary TV Start			95.4	7071	6721	95.4				95.8
Interval between TVI and TV			95.4	0	270	95.4				97.5
Boundary TVI End			95.4	7149	6892	95.4				99.1
Interval Duration TVI			95.4	632	946	95.4				98
Span Span of TVI			95.4	590	826	95.4				97.9
R_Date TVI OXA-20857	7612	7432	95.4	7610	7431	95.4		95.5	97.3	98.8
R_Date TVI OXA-20856	7250	6981	95.4	7253	6991	95.4		99.5	96.5	98.2
R_Date TVI OXA-20855	7920	7684	95.4	7841	7668	95.4		102.8	96.2	97.8
R_Date TVI OXA-20854	7918	7682	95.4	7832	7672	95.4		105.8	97.4	98.2
R_Date TVICDF_113-MUSE21094	7827	7671	95.4	7793	7621	95.4		103.5	98.1	98.8
R_Date TVI88-MUSE21086	7832	7675	95.4	7826	7665	95.4		105.5	97.7	98.5
R_Date TVI86-MUSE21085	7931	7730	95.4	7870	7673	95.4		65.3	94.4	96.6

R_Date TVI83-MUSE21084	7161	6961	95.4	7237	6959	95.4		101.6	95.5	98.6
R_Date TVI82-MUSE21064	7263	7025	95.4	7262	7026	95.4		94.8	97.9	98.6
R_Date TVI81-MUSE21063	7268	7031	95.4	7267	7025	95.4		95.4	97.5	98.6
Phase TVI			95.4							
Boundary TVI Start			95.4	7891	7727	95.4				94.4
Interval between TVII and TVI			95.4	0	112	95.4				97.1
Boundary TVII End			95.4	7943	7744	95.4				89.2
Interval Duration TVII			95.4	147	1231	95.4				73.6
Span Span of TVII			95.4	119	882	95.4				72.4
R_Date TVII72-MUSE21088	7917	7690	95.4	8318	7746	95.4		51.7	78.4	92.1
R_Date TVII1-MUSE21087	8748	8543	95.4	8720	7833	95.4		56.8	59.4	81.9
R_Date TVII42-MUSE21072	8323	8037	95.4	8317	8029	95.4		85.3	97.4	95.6
R_Date TVII71-MUSE21071	8175	8028	95.4	8176	8019	95.4		100.3	97.9	97.8
R_Date TVII74-MUSE21062	7975	7842	95.4	8009	7838	95.4		94.5	96.8	97.3
R_Date TVII69-MUSE21061	7777	7611	95.4	8577	7752	95.4		5.4	8.2	56.3
Phase TVII			95.4			95.4				
Boundary TVII Start			95.4	9037	8048	95.4				66.9
Sequence Telarmachay			95.4			95.4				
U(0,4)	3.98986e-17	4	95.4	2.272	3.108	95.4		100		11.5
T(5)	-2.65	2.65	95.4			95.4				81.4

Outlier_Model General			95.4	-1786	2218	95.4					36.6
Mix_Curves Mixed	9.29812e-16	100	95.4	35.2	100	95.4		100			99.5
Curve SHCal20			95.4								
Curve IntCal20			95.4								

Appendix 5: Dates ^{14}C of Junin's sites available in literature - Pachamachay (Rick 1980; Rademaker and Moore 2019), Panaulauca (Moore 1998; Rick and Moore 1999; Rademaker and Moore 2019; Salcedo Camacho and Marcos 2019), Uchkumachay (Kaulicke 1999; Salcedo Camacho and Marcos 2019) and Cuchimachay (Salcedo Camacho and Marcos 2019) - and their calibration with the “SHcal20” curve (Hogg et al. 2020) in BP.

Reference	Site	Samples lab code	Layer	^{14}C age (BP)		Calibrated range		%
				raw age	Error	Start (BP)	End (BP)	
Lavallee et al. 1995, Wheeler 2000	cuchimachay	Ny-237	III A	5580	80	6539	6122	95.45
Rademaker and Moore 2019/Moore 1998	panaulauca	WSU-2940	phase 1	9650	145	11 266	10512	95.45
Rademaker and Moore 2019/Moore 1998	panaulauca	Beta-7724	phase 2a	8350	140	9549	8814	95.45
Rademaker and Moore 2019/Moore 1998	panaulauca	WSU-2939	phase 2b	7650	95	8594	8194	95.45
Rademaker and Moore 2019/Moore 1998	panaulauca	WSU-3002	phase 3	5990	90	7153	6505	95.45
Rademaker and Moore 2019/Moore 1998	panaulauca	WSU-2938	phase 4	5135	75	5999	5605	95.45
Salcedo Camacho and Marcos 2019	panaulauca	WSU-3001	18 phase 5	4040	60	4801	4250	95.45

Salcedo Camacho and Marcos 2019	panaulauca	WSU-3000	16 phase 5	3630	90	4218	3640	95.45
Moore 1998	panaulauca	WSU-2998	phase 7	2680	95	2992	2373	95.45
Moore 1998	panaulauca	WSU-2997	phase 8	1095	65	1177	794	95.45
Moore 1998	panaulauca	WSU-2996	phase 8	750	50	728	559	95.45
Salcedo Camacho and Marcos 2019/Kaulicke 1999	uchkumachay-tilarnioc	Oxa-510	5	6670	120	7700	7275	95.45
Rick 1980; Rademaker and Moore 2019; Salcedo Camacho and Marcos 2019	pachamachay	UCLA-2118A	32	11800	930	16997	11630	95.45
Rick 1980; Rademaker and Moore 2019; Salcedo Camacho and Marcos 2019	pachamachay	UCR-554	31	9010	285	11069	9456	95.45
Rick 1980; Rademaker and Moore 2019; Salcedo Camacho and Marcos 2019	pachamachay	UCR-555	28 II	8125	280	9659	8362	95.45
Rick 1980; Rademaker and Moore 2019; Salcedo Camacho and Marcos 2019	pachamachay	UCR-557	25 III	6580	255	7933	6890	95.45
Rick 1980; Rademaker and Moore 2019; Salcedo Camacho and Marcos 2019	pachamachay	UCLA-2118D	23 III	5080	60	5917	5605	95.45
Rick 1980; Rademaker and Moore 2019; Salcedo Camacho and Marcos 2019	pachamachay	UCR-556	19 IV	6100	250	7460	6354	95.45
Rick 1980; Rademaker and Moore 2019; Salcedo Camacho and Marcos 2019	pachamachay	UCLA-2118B	17 V	3800	60	4401	3928	95.45
Rick 1980; Rademaker and Moore 2019;	pachamachay	LJ-3286	21 VI	3660	60	4146	3724	95.45

Salcedo Camacho and Marcos 2019								
Rick 1980; Rademaker and Moore 2019; Salcedo Camacho and Marcos 2019	pachamachay	UCLA-2118C	13 VI	3640	60	4137	3719	95.45

Appendix 6: codes used for the different models presented in the manuscript, in the latest version of Oxcal software (v4.4):

- a. code used for the Radiocarbon age calibration of the charcoal from Lavallée and Julien (1980); Lavallée et al. (1985) and SAC bones (Metcalf et al. 2016) with the “Shcal20” curve (Hogg et al. 2020) in BP:

Plot()

```
{
Curve("SHCal20","shcal20.14c");
Phase ("Telarmachay TVII")
{
R_Date("VIIb Pucp-1825", 12040, 120);
R_Date("VIIb Lv-1279", 8810, 65);
R_Date("VIIa Lv-1193", 7620, 60);
R_Date("VIIa Gif-5389", 7250, 140);
R_Date("VIIa Lv-1278", 7140, 60);
};
Phase ("Telarmachay TVI")
{
R_Date("VIa Lv-1277", 7150, 90);
R_Date("VIa Gif-5388", 5580, 120);
R_Date("VIa Gif-5394", 5320, 110);
R_Date("VIa Gif-5390", 4220, 110);
};
Phase ("Telarmachay TV")
{
R_Date("Vc Gif-5392", 6780, 130);
R_Date("Vc Lv-1192", 6110, 80);
R_Date("Vb Lv-1134", 5700, 65);
R_Date("Va Gif-5046", 5370, 110);
R_Date("Vb-c Gif-5391", 5320, 120);
R_Date("Va Gif-5047", 5190, 110);
R_Date("Vc Lv-1276", 5000, 80);
R_Date("Va-b Lv-1190", 4910, 80);
R_Date("Va Gif-5393", 4430, 70);
};
Phase ("Telarmachay TIV")
{
R_Date("IVa Gif-4837", 4470, 110);
R_Date("IVc Gif-5045", 4420, 110);
}
```

```

R_Date("IVa Gif-4834", 3910, 110);
R_Date("IVa Gif-4836", 3700, 100);
R_Date("IVa Gif-4835", 3680, 100);
};

Phase ("Telarmachay TIII")
{
R_Date("IIIinf Gif-4189", 3470, 100);
R_Date("IIIsup Gif-4188", 3410, 100);
};

Phase ("Telarmachay TII")
{
R_Date("IIinf Gif-4187", 2600, 90);
R_Date("IImoy Gif-3773", 2280, 100);
R_Date("IIsup Gif-3774", 2120, 100);
R_Date("IIsup Gif-3772", 2190, 100);
};

};


```

- b. code used for the Radiocarbon age obtained on camelid bone collagen from Telarmachay (Cal BP 2 sigmas) and calibrated dates (Cal BP) with the (SHcal20) curve (Hogg et al. 2020):

```

Plot()
{
Curve("SHCal20","shcal20.14c");
Phase ("Telarmachay TVII")
{
R_Date("TVII69-MUSE21061", 6870, 30);
R_Date("TVII74-MUSE21062", 7110, 30);
R_Date("TVII71-MUSE21071", 7320, 30);
R_Date("TVII42-MUSE21072", 7395, 30);
R_Date("TVII1-MUSE21087", 7860, 30);
R_Date("TVII72-MUSE21088", 6975, 30);
};

Phase ("Telarmachay TVI")
{
R_Date("TVI81-MUSE21063", 6290, 30);
R_Date("TVI82-MUSE21064", 6280, 30);
R_Date("TVI83-MUSE21084", 6185, 30);
R_Date("TVI86-MUSE21085", 7010, 30);
R_Date("TVI88-MUSE21086", 6935, 30);
R_Date("TVICDF_113-MUSE21094", 6920, 30);
R_Date("TVI OXA-20854", 6965, 40);
R_Date("TVI OXA-20855", 6970, 40);
R_Date("TVI OXA-20856", 6220, 40);
R_Date("TVI OXA-20857", 6690, 40);
};

Phase ("Telarmachay TV")
{
R_Date("TV34-MUSE21065", 4160, 25);
R_Date("TV24-MUSE21066", 5935, 25);
R_Date("TV9-MUSE21081", 5780, 30);
R_Date("TV12-MUSE21082", 5435, 25);

```

```

R_Date("TV17-MUSE21083", 5875, 25);
R_Date("TVCDF_110-MUSE21093", 6095, 30);
};

Phase ("Telarmachay TIV")
{
R_Date("TIV42-MUSE21068", 5855, 30);
R_Date("TIV37-MUSE21078", 4240, 25);
R_Date("TIV38-MUSE21079", 5395, 30);
R_Date("TIV40-MUSE21080", 4750, 30);
R_Date("TIVCDF_105_1-MUSE21089", 5210, 30);
R_Date("TIVCDF_105_2-MUSE21090", 5120, 30);
R_Date("TIVCDF_109_1-MUSE21091", 5215, 30);
R_Date("TIVCDF_109_2-MUSE21092", 5040, 25);
};

Phase ("Telarmachay TIII")
{
R_Date("TIII59-MUSE21069", 5140, 30);
R_Date("TIII56-MUSE21075", 3545, 25);
R_Date("TIII57-MUSE21076", 3920, 25);
R_Date("TIII50-MUSE21077", 4055, 25);
};

Phase ("Telarmachay TII")
{
R_Date("TII23-MUSE21070", 3900, 25);
R_Date("TII7-MUSE21073", 4065, 25);
R_Date("TII47-MUSE21074", 3420, 25);
};

};

```

- c. “v0” – first code of the phases modelized (Bayesian model) used for the Radiocarbon age obtained on camelid bone collagen from Telarmachay (Cal BP 2 sigmas) and calibrated dates (Cal BP) with the (SHcal20) curve (Hogg et al. 2020):

```

Options()
{
kIterations=10;
Resolution=1;
};

Plot()
{
Curve("SHCal20","shcal20.14c");
Sequence("Telarmachay")
{
Boundary("TVII Start");
Phase("TVII")
{
R_Date("TVII69-MUSE21061", 6870, 29);
R_Date("TVII74-MUSE21062", 7111, 29);
R_Date("TVII71-MUSE21071", 7319, 29);
R_Date("TVII42-MUSE21072", 7395, 29);
R_Date("TVII1-MUSE21087", 7859, 30);
R_Date("TVII72-MUSE21088", 6974, 29);
}
}
}
```

```

Span("Span of TVII");
Interval("Duration TVII");
};

Boundary("TVII End");
Interval("between TVII and TVI");
Boundary("TVI Start");
Phase("TVI")
{
R_Date("TVI81-MUSE21063", 6290, 28);
R_Date("TVI82-MUSE21064", 6278, 28);
R_Date("TVI83-MUSE21084", 6187, 28);
R_Date("TVI86-MUSE21085", 7012, 29);
R_Date("TVI88-MUSE21086", 6937, 29);
R_Date("TVI-MUSE21094", 6919, 30);
R_Date("TVI OXA-20854", 6965, 40);
R_Date("TVI OXA-20855", 6970, 40);
R_Date("TVI OXA-20856", 6220, 40);
R_Date("TVI OXA-20857", 6690, 40);
Span("Span of TVI");
Interval("Duration TVI");
};

Boundary("TVI End");
Interval("between TVI and TV");
Boundary("TV Start");
Phase("TV")
{
R_Date("TV34-MUSE21065", 4160, 25);
R_Date("TV24-MUSE21066", 5936, 27);
R_Date("TV9-MUSE21081", 5782, 28);
R_Date("TV12-MUSE21082", 5436, 27);
R_Date("TV17-MUSE21083", 5877, 27);
Span("Span of TV");
Interval("Duration TV");
};

Boundary("TV End");
Interval("between TV and TIV");
Boundary("TIV Start");
Phase("TIV")
{
R_Date("TIV42-MUSE21068", 5860, 29);
R_Date("TIV37-MUSE21078", 4247, 26);
R_Date("TIV38-MUSE21079", 5396, 29);
R_Date("TIV40-MUSE21080", 4746, 28);
R_Date("TIV-MUSE21089", 5211, 28);
R_Date("TIV-MUSE21090", 5136, 28);
R_Date("TIV-MUSE21091", 5213, 29);
R_Date("TIV-MUSE21092", 5041, 28);
Span("Span of TIV");
Interval("Duration TIV");
};

Boundary("TIV End");
Interval("between TIV and TIII");
Boundary("TIII Start");
Phase("TIII")
{

```

```

R_Date("TIII59-MUSE21069", 5146, 28);
R_Date("TIII56-MUSE21075", 3550, 27);
R_Date("TIII57-MUSE21076", 3929, 27);
R_Date("TIII50-MUSE21077", 4057, 26);
Span("Span of TIII");
Interval("Duration TIII");
};

Boundary("TIII End");
Interval("between TIII and TII");
Boundary("TII Start");
Phase("TII")
{
R_Date("TII23-MUSE21070", 3905, 26);
R_Date("TII7-MUSE21073", 4068, 26);
R_Date("TII47-MUSE21074", 3423, 25);
Span("Span of TII");
Interval("Duration TII");
};

Boundary("TII End");
};

};


```

- **d. code of the phases modelized (“second” Bayesian model) used for the Radiocarbon age obtained on camelid bone collagen from Telarmachay (Cal BP 2 sigmas) and calibrated dates (Cal BP) with the (SHcal20) curve (Hogg et al. 2020):**

```

Options()
{
kIterations=10;
Resolution=1;
};

Plot()
{
Curve("SHCal20","shcal20.14c");
Outlier_Model("General",T(5),U(0,4),"t");
Sequence("Telarmachay")
{
Boundary("TVII Start");
Phase("TVII")
{
R_Date("TVII69-MUSE21061", 6870, 30)
{
Outlier("General", 0.05);
};
R_Date("TVII74-MUSE21062", 7110, 30)
{
Outlier("General", 0.05);
};
R_Date("TVII71-MUSE21071", 7320, 30)
{
Outlier("General", 0.05);
};
R_Date("TVII42-MUSE21072", 7395, 30)


```

```
{  
    Outlier("General", 0.05);  
};  
R_Date("TVII1-MUSE21087", 7860, 30)  
{  
    Outlier("General", 0.05);  
};  
R_Date("TVII72-MUSE21088", 6975, 30)  
{  
    Outlier("General", 0.05);  
};  
Span("Span of TVII");  
Interval("Duration TVII");  
};  
Boundary("TVII End");  
Interval("between TVII and TVI");  
Boundary("TVI Start");  
Phase("TVI")  
{  
    R_Date("TVI81-MUSE21063", 6290, 30)  
    {  
        Outlier("General", 0.05);  
    };  
    R_Date("TVI82-MUSE21064", 6280, 30)  
    {  
        Outlier("General", 0.05);  
    };  
    R_Date("TVI83-MUSE21084", 6185, 30)  
    {  
        Outlier("General", 0.05);  
    };  
    R_Date("TVI86-MUSE21085", 7010, 30)  
    {  
        Outlier("General", 0.05);  
    };  
    R_Date("TVI88-MUSE21086", 6935, 30)  
    {  
        Outlier("General", 0.05);  
    };  
    R_Date("TVICDF_113-MUSE21094", 6920, 30)  
    {  
        Outlier("General", 0.05);  
    };  
    R_Date("TVI OXA-20854", 6965, 40)  
    {  
        Outlier("General", 0.05);  
    };  
    R_Date("TVI OXA-20855", 6970, 40)  
    {  
        Outlier("General", 0.05);  
    };  
    R_Date("TVI OXA-20856", 6220, 40)  
    {  
        Outlier("General", 0.05);  
    };
```

```

R_Date("TVI OXA-20857",6690, 40)
{
  Outlier("General", 0.05);
};
Span("Span of TVI");
Interval("Duration TVI");
};
Boundary("TVI End");
Interval("between TVI and TV");
Boundary("TV Start");
Phase("TV")
{
  R_Date("TV34-MUSE21065", 4160, 25)
  {
    Outlier("General", 0.05);
  };
  R_Date("TV24-MUSE21066", 5935, 25)
  {
    Outlier("General", 0.05);
  };
  R_Date("TV9-MUSE21081", 5780, 30)
  {
    Outlier("General", 0.05);
  };
  R_Date("TV12-MUSE21082", 5435, 25)
  {
    Outlier("General", 0.05);
  };
  R_Date("TV17-MUSE21083", 5875, 25)
  {
    Outlier("General", 0.05);
  };
  R_Date("TVCDF_110-MUSE21093", 6095, 30)
  {
    Outlier("General", 0.05);
  };
  Span("Span of TV");
  Interval("Duration TV");
};
Boundary("TV End");
Interval("between TV and TIV");
Boundary("TIV Start");
Phase("TIV")
{
  R_Date("TIV42-MUSE21068", 5855, 30)
  {
    Outlier("General", 0.05);
  };
  R_Date("TIV37-MUSE21078", 4240, 25)
  {
    Outlier("General", 0.05);
  };
  R_Date("TIV38-MUSE21079", 5395, 30)
  {
    Outlier("General", 0.05);
  };
}

```

```

};

R_Date("TIV40-MUSE21080", 4750, 30)
{
    Outlier("General", 0.05);
};

R_Date("TIVCDF_105_1-MUSE21089", 5210, 30)
{
    Outlier("General", 0.05);
};

R_Date("TIVCDF_105_2-MUSE21090", 5120, 30)
{
    Outlier("General", 0.05);
};

R_Date("TIVCDF_109_1-MUSE21091", 5215, 30)
{
    Outlier("General", 0.05);
};

R_Date("TIVCDF_109_2-MUSE21092", 5040, 25)
{
    Outlier("General", 0.05);
};

Span("Span of TIV");
Interval("Duration TIV");
};

Boundary("TIV End");
Interval("between TIV and TIII-II");
Boundary("TIII-II Start");
Phase("TIII-II")
{
    R_Date("TIII59-MUSE21069", 5140, 30)
    {
        Outlier("General", 0.05);
    };

    R_Date("TIII56-MUSE21075", 3545, 25)
    {
        Outlier("General", 0.05);
    };

    R_Date("TIII57-MUSE21076", 3920, 25)
    {
        Outlier("General", 0.05);
    };

    R_Date("TIII50-MUSE21077", 4055, 25)
    {
        Outlier("General", 0.05);
    };

    R_Date("TII23-MUSE21070", 3900, 25)
    {
        Outlier("General", 0.05);
    };

    R_Date("TII7-MUSE21073", 4065, 25)
    {
        Outlier("General", 0.05);
    };

    R_Date("TII47-MUSE21074", 3420, 25)
    {

```

```

    Outlier("General", 0.05);
};

Span("Span of TII-II");
Interval("Duration TII-II");
};

Boundary("TII-II End");
};

};

```

e. code used for the radiocarbon age of camelid bone collagen from Telarmachay (Cal BP 2 sigmas) and calibrated with the mixed curve IntCal20 (Reimer et al. 2020) and SHcal20 (Hogg et al. 2020) approach (Buck 2004; Ogburn 2012; Marsh et al. 2017; Marsh et al. 2018):

```

Plot()
{
  Curve("IntCal20","IntCal20.14c");
  Curve("SHCal20","shcal20.14c");
  Mix_Curve("Mixed","IntCal20","SHCal20",U(0,100));
  Phase ("Telarmachay TVII")
  {
    R_Date("TVII69-MUSE21061", 6870, 30);
    R_Date("TVII74-MUSE21062", 7110, 30);
    R_Date("TVII71-MUSE21071", 7320, 30);
    R_Date("TVII42-MUSE21072", 7395, 30);
    R_Date("TVII1-MUSE21087", 7860, 30);
    R_Date("TVII72-MUSE21088", 6975, 30);
  };
  Phase ("Telarmachay TVI")
  {
    R_Date("TVI81-MUSE21063", 6290, 30);
    R_Date("TVI82-MUSE21064", 6280, 30);
    R_Date("TVI83-MUSE21084", 6185, 30);
    R_Date("TVI86-MUSE21085", 7010, 30);
    R_Date("TVI88-MUSE21086", 6935, 30);
    R_Date("TVICDF_113-MUSE21094", 6920, 30);
    R_Date("TVI OXA-20854", 6965, 40);
    R_Date("TVI OXA-20855", 6970, 40);
    R_Date("TVI OXA-20856", 6220, 40);
    R_Date("TVI OXA-20857", 6690, 40);
  };
  Phase ("Telarmachay TV")
  {
    R_Date("TV34-MUSE21065", 4160, 25);
    R_Date("TV24-MUSE21066", 5935, 25);
    R_Date("TV9-MUSE21081", 5780, 30);
    R_Date("TV12-MUSE21082", 5435, 25);
    R_Date("TV17-MUSE21083", 5875, 25);
    R_Date("TVCDF_110-MUSE21093", 6095, 30);
  };
  Phase ("Telarmachay TIV")
  {
    R_Date("TIV42-MUSE21068", 5855, 30);
    R_Date("TIV37-MUSE21078", 4240, 25);
  };
}

```

```

R_Date("TIV38-MUSE21079", 5395, 30);
R_Date("TIV40-MUSE21080", 4750, 30);
R_Date("TIVCDF_105_1-MUSE21089", 5210, 30);
R_Date("TIVCDF_105_2-MUSE21090", 5120, 30);
R_Date("TIVCDF_109_1-MUSE21091", 5215, 30);
R_Date("TIVCDF_109_2-MUSE21092", 5040, 25);
};

Phase ("Telarmachay TIII")
{
    R_Date("TIII59-MUSE21069", 5140, 30);
    R_Date("TIII56-MUSE21075", 3545, 25);
    R_Date("TIII57-MUSE21076", 3920, 25);
    R_Date("TIII50-MUSE21077", 4055, 25);
};

Phase ("Telarmachay TII")
{
    R_Date("TII23-MUSE21070", 3900, 25);
    R_Date("TII7-MUSE21073", 4065, 25);
    R_Date("TII47-MUSE21074", 3420, 25);
};
};

```

- f. code of the phases modelized (Bayesian model) used for the Radiocarbon age obtained on camelid bone collagen from Telarmachay (Cal BP 2 sigmas) and calibrated dates (Cal BP) with the mixed curve IntCal20 (Reimer et al. 2020) and SHcal20 (Hogg et al. 2020) approach (Buck 2004; Ogburn 2012; Marsh et al. 2017; Marsh et al. 2018):

```

Options()
{
    kIterations=10;
    Resolution=1;
};

Plot()
{
    Curve("IntCal20","IntCal20.14c");
    Curve("SHCal20","shcal20.14c");
    Mix_Curve("Mixed","IntCal20","SHCal20",U(0,100));
    Outlier_Model("General",T(5),U(0,4),"t");
    Sequence("Telarmachay")
    {
        Boundary("TVII Start");
        Phase("TVII")
        {
            R_Date("TVII69-MUSE21061", 6870, 30)
            {
                Outlier("General", 0.05);
            };
            R_Date("TVII74-MUSE21062", 7110, 30)
            {
                Outlier("General", 0.05);
            };
            R_Date("TVII71-MUSE21071", 7320, 30)
        };
    };
};

```

```

{
Outlier("General", 0.05);
};

R_Date("TVII42-MUSE21072", 7395, 30)
{
Outlier("General", 0.05);
};

R_Date("TVII1-MUSE21087", 7860, 30)
{
Outlier("General", 0.05);
};

R_Date("TVII72-MUSE21088", 6975, 30)
{
Outlier("General", 0.05);
};

Span("Span of TVII");
Interval("Duration TVII");
};

Boundary("TVII End");
Interval("between TVII and TVI");
Boundary("TVI Start");
Phase("TVI")
{
    R_Date("TVI81-MUSE21063", 6290, 30)
    {
        Outlier("General", 0.05);
    };

    R_Date("TVI82-MUSE21064", 6280, 30)
    {
        Outlier("General", 0.05);
    };

    R_Date("TVI83-MUSE21084", 6185, 30)
    {
        Outlier("General", 0.05);
    };

    R_Date("TVI86-MUSE21085", 7010, 30)
    {
        Outlier("General", 0.05);
    };

    R_Date("TVI88-MUSE21086", 6935, 30)
    {
        Outlier("General", 0.05);
    };

    R_Date("TVICDF_113-MUSE21094", 6920, 30)
    {
        Outlier("General", 0.05);
    };

    R_Date("TVI OXA-20854", 6965, 40)
    {
        Outlier("General", 0.05);
    };

    R_Date("TVI OXA-20855", 6970, 40)
    {
        Outlier("General", 0.05);
    };
}

```

```

R_Date("TVI OXA-20856",6220, 40)
{
  Outlier("General", 0.05);
};
R_Date("TVI OXA-20857",6690, 40)
{
  Outlier("General", 0.05);
};
Span("Span of TVI");
Interval("Duration TVI");
};

Boundary("TVI End");
Interval("between TVI and TV");
Boundary("TV Start");
Phase("TV")
{
  R_Date("TV34-MUSE21065", 4160, 25)
  {
    Outlier("General", 0.05);
  };
  R_Date("TV24-MUSE21066", 5935, 25)
  {
    Outlier("General", 0.05);
  };
  R_Date("TV9-MUSE21081", 5780, 30)
  {
    Outlier("General", 0.05);
  };
  R_Date("TV12-MUSE21082", 5435, 25)
  {
    Outlier("General", 0.05);
  };
  R_Date("TV17-MUSE21083", 5875, 25)
  {
    Outlier("General", 0.05);
  };
  R_Date("TVCDF_110-MUSE21093", 6095, 30)
  {
    Outlier("General", 0.05);
  };
  Span("Span of TV");
  Interval("Duration TV");
};

Boundary("TV End");
Interval("between TV and TIV");
Boundary("TIV Start");
Phase("TIV")
{
  R_Date("TIV42-MUSE21068", 5855, 30)
  {
    Outlier("General", 0.05);
  };
  R_Date("TIV37-MUSE21078", 4240, 25)
  {
    Outlier("General", 0.05);
  };
}

```

```

};

R_Date("TIV38-MUSE21079", 5395, 30)
{
Outlier("General", 0.05);
};

R_Date("TIV40-MUSE21080", 4750, 30)
{
Outlier("General", 0.05);
};

R_Date("TIVCDF_105_1-MUSE21089", 5210, 30)
{
Outlier("General", 0.05);
};

R_Date("TIVCDF_105_2-MUSE21090", 5120, 30)
{
Outlier("General", 0.05);
};

R_Date("TIVCDF_109_1-MUSE21091", 5215, 30)
{
Outlier("General", 0.05);
};

R_Date("TIVCDF_109_2-MUSE21092", 5040, 25)
{
Outlier("General", 0.05);
};

Span("Span of TIV");
Interval("Duration TIV");

};

Boundary("TIV End");
Interval("between TIV and TIII-II");
Boundary("TIII-II Start");
Phase("TIII-II")
{

R_Date("TIII59-MUSE21069", 5140, 30)
{
Outlier("General", 0.05);
};

R_Date("TIII56-MUSE21075", 3545, 25)
{
Outlier("General", 0.05);
};

R_Date("TIII57-MUSE21076", 3920, 25)
{
Outlier("General", 0.05);
};

R_Date("TIII50-MUSE21077", 4055, 25)
{
Outlier("General", 0.05);
};

R_Date("TII23-MUSE21070", 3900, 25)
{
Outlier("General", 0.05);
};

R_Date("TII7-MUSE21073", 4065, 25)
{

```

```

    Outlier("General", 0.05);
};

R_Date("TII47-MUSE21074", 3420, 25)
{
    Outlier("General", 0.05);
};

Span("Span of TII-II");
Interval("Duration TII-II");
};

Boundary("TII-II End");
};
};

```

Appendix 7: comparison for the Telarmachay chronostratigraphies by layers:

- “Charcoal chronology”: based on charcoal radiocarbon ages (Lavallée and Julien 1980; Lavallée et al. 1985) and SAC bones (Metcalf et al. 2016) after their calibration with the “Shcal20” curve (Hogg et al. 2020) in BP.
- “Bones chronology”: based on the Bayesian age model using a t-type outlier model method with prior probabilities set at 0.05. The model is based camelid radiocarbon ages and calibrated using the (SHcal20) curve (Hogg et al. 2020).

Layer number	« First » chronology		« New » chronology	
	Boundary start	Boundary end	Boundary start	Boundary end
III-II	4.0-3.5	2.3-1.8	5.2-4.4	3.8-3.0
IV	5.4-4.8	4.3-3.7	6.4-6.0	5.8-4.5
V	7.9-7.4	5.3-4.8	7.1-6.8	6.6-6.0
VI	8.2-7.7	5.0-4.4	7.9-7.7	7.1-6.9
VII	14.2-13.5	8.3-7.8	9.1 - 8.0	7.9 - 7.7